Computer Modeling in Engineering & Sciences

Tech Science Press

Doi:10.32604/cmes.2025.064900

ARTICLE

# Design of Chaos Induced Aquila Optimizer for Parameter Estimation of Electro-Hydraulic Control System

**Khizer Mehmood[1], Naveed Ishtiaq Chaudhary[2,*], Zeshan Aslam Khan[3], Khalid Mehmood Cheema[4], Muhammad Asif Zahoor Raja[2], Sultan S. Alshamrani[5] and Kaled M. Alshmrany[6]**

[1]Department of Electrical and Computer Engineering, International Islamic University, Islamabad, 44000, Pakistan
[2]Future Technology Research Center, National Yunlin University of Science and Technology, Yunlin, 64002, Taiwan
[3]International Graduate School of Artificial Intelligence, National Yunlin University of Science and Technology, Yunlin, 64002, Taiwan
[4]Department of Electronic Engineering, Fatima Jinnah Women University, Rawalpindi, 46000, Pakistan
[5]Department of Information Technology, College of Computer and Information Technology, Taif University, Taif, 21944, Saudi Arabia
[6]Institute of Public Administration, Jeddah, 21944, Saudi Arabia

*Corresponding Author: Naveed Ishtiaq Chaudhary. Email: chaudni@yuntech.edu.tw

Received: 27 February 2025; Accepted: 23 April 2025; Published: 30 May 2025

**ABSTRACT:** Aquila Optimizer (AO) is a recently proposed population-based optimization technique inspired by Aquila's behavior in catching prey. AO is applied in various applications and its numerous variants were proposed in the literature. However, chaos theory has not been extensively investigated in AO. Moreover, it is still not applied in the parameter estimation of electro-hydraulic systems. In this work, ten well-defined chaotic maps were integrated into a narrowed exploitation of AO for the development of a robust chaotic optimization technique. An extensive investigation of twenty-three mathematical benchmarks and ten IEEE Congress on Evolutionary Computation (CEC) functions shows that chaotic Aquila optimization techniques perform better than the baseline technique. The investigation is further conducted on parameter estimation of an electro-hydraulic control system, which is performed on various noise levels and shows that the proposed chaotic AO with Piecewise map (CAO6) achieves the best fitness values of 2.873E−05, 1.014E−04, and 8.728E−03 at noise levels 1.300E−03, 1.300E−02, and 1.300E−01, respectively. Friedman test for repeated measures, computational analysis, and Taguchi test reflect the superiority of CAO6 against the state of the arts, demonstrating its potential for addressing various engineering optimization problems. However, the sensitivity to parameter tuning may limit its direct application to complex optimization scenarios.

**KEYWORDS:** Aquila optimizer; electro-hydraulic control system; chaos theory; autoregressive model

## 1 Introduction

Optimization techniques (OT) are applied in solving different problems related to science and engineering, such as wireless sensor networks [1], an electrically stimulated muscle model [2], leukemia cancer classification [3], nonlinear system identification [4], flow shop scheduling [5], feature selection [6], power system harmonics [7], agriculture [8], and renewable energy [9]. Machine learning assisted OT was also used for numerous applications, such as antenna design [10,11] and geometry [12], aircraft trajectories [13], and electronic packages and materials [14]. OT can be classified as swarm optimization techniques (SOT),

evolutionary optimization techniques (EOT), physics-based optimization techniques (PBOT), and human-based optimization techniques (HBOT). In recent years, various optimizations have been proposed in each category. Some of them are given in Table 1.

**Table 1:** Classification of OT

| Category | Techniques |
|---|---|
| SOT | Particle Swarm Optimization (PSO) [15]<br>Monarch Butterfly Algorithm [16]<br>Reptile Search Algorithm [17]<br>Whale Optimization Algorithm [18]<br>Synergistic Swarm Optimization Algorithm (SSOA) [19] |
| EOT | Differential Evolution (DE) [20]<br>Artificial Circulation System Algorithm (ACSA) [21]<br>Biogeography-Based Optimization (BBO) [22]<br>Earthworm Optimization Algorithm [23]<br>Moth Search Algorithm [24] |
| PBOT | Arithmetic Optimization Algorithm (AOA) [25]<br>Sinh Cosh Optimizer (SCHO) [26]<br>Multi-Verse Optimizer (MVO) [27]<br>Gravitational Search Algorithm (GSA) [28]<br>Henry Gas Solubility Optimization (HGSO) [29] |
| HBOT | Political Optimizer (PO) [30]<br>Stock Exchange Trading Optimization Algorithm(SETOA) [31]<br>Teaching Learning Based Optimization (TLBO) [32]<br>Heap-Based Optimizer (HBO) [33]<br>Future Search Algorithm (FSA) [34] |

The comparison between the advantages and disadvantages of some of the OT is given in Table 2.

**Table 2:** Advantages and disadvantages of OT

| OT | Advantages | Disadvantages |
|---|---|---|
| Aquila optimizer | Few tuning parameters | Lacks extensive testing for diverse applications |
| Arithmetic optimization algorithm | Suitable for parameter-free problems | Premature convergence |
| Reptile search algorithm | Suitable for parameter-constrained problems | Slow convergence |
| Whale optimization algorithm | Few tuned parameters | Poor scalability |

Aquila Optimizer (AO) [35] is recently proposed OT, and its various variants were available in the literature [36] with applications in diversified fields such as optimal power flow [37], biomedical [38], text-to-speech conversion [39], anomaly detection [40], wireless sensor networks [41], generative adversarial

networks [42], power transformers [43], fraud detection [44], autoregressive models [45], agriculture [46], distributed energy systems [47], image segmentation [48], vehicle cruise control system [49], automatic voltage regulator [50], Unmanned Aerial Vehicles [51], air fuel ratio system control [52], and PV systems [53]. Various improved variants of AO were also proposed such as fractional order chaotic oscillator-based AO [54], binary AO [55], local search enhanced AO [56], reinforcement learning based AO [57], chaotic mapping-based AO [58], adaptive AO [59], and chaotic opposition learning based AO [60].

Parameter identification is critical for precisely modeling electro-hydraulic control systems, as it includes defining system-specific parameters like viscosity, valve coefficients, and actuator dynamics to confirm accurate control [61]. Various techniques were proposed in the literature for its representation [62–64]. Autoregressive models are widely applied for the representation of linear and nonlinear systems [65]. For its identification, various techniques were present in the literature, such as the two-stage gradient [66], hybrid neural fuzzy [67], SOT [68], and momentum gradient descent [69]. Accurate identification improves the consistency and effectiveness of electro-hydraulic systems, empowering better control of various industrial systems [70].

In this work, an improved variant of AO, namely chaotic Aquila optimizer (CAO), is proposed by integrating the chaos theory [71–73] through ten well-known chaotic maps into narrow exploitation. Chaotic maps in AO are motivated by their ability to enhance exploration and exploitation dynamics, leveraging chaotic maps to introduce randomness. CAO is further applied to the parameter estimation of the electro-hydraulic control system. The performance of CAO is compared with the arithmetic optimization algorithm (AOA) [25], reptile search algorithm (RSA) [17] and whale optimization algorithm (WOA) [18]. The prominent features of this research work are:

- Integration of chaos theory with SOT-based AO is proposed for parameter estimation of the electro-hydraulic control system.
- The integration of chaotic maps in the narrowed exploitation of AO provides better performance than its baseline technique.
- Friedman test for repeated measures, convergence analysis, computational analysis, and Taguchi test recommend the precision of the proposed CAO in comparison with the state of the art.

The workflow is as follows: Section 2 comprises mathematical models of AO, CAO, and fitness definition. Section 3 provides an analysis of CEC and benchmark functions. Section 4 presents the investigation on the electro-hydraulic control system. Section 5 provides the concluding remarks.

## 2 Methodology

This section provides mathematical model of Aquila Optimizer (AO), Chaotic Aquila Optimizer (CAO), fitness evaluation, and pseudo codes.

### *2.1 Aquila Optimizer (AO)*

AO is a nature-inspired optimization technique involving four hunting strategies to catch prey. It starts with population initialization generated randomly for the upper and lower bounds of the given problem as shown in Eqs. (1) and (2).

$$U = \begin{bmatrix} u_{1,1} & \cdots & u_{1,Dim} \\ \vdots & \ddots & \vdots \\ u_{P_s,1} & \cdots & u_{P_s,Dim} \end{bmatrix} \tag{1}$$

$$U_{i,j} = \text{rand}\left(Ub_j - Lb_j\right) + Lb_j, i = 1, 2 \ldots p_s, j = 1, 2 \ldots Dim \tag{2}$$

here Ub, Lb, $p_s$ and Dim are upper bound, lower bound, population size and decision variables, respectively. Its mathematical formulation includes expanded exploration ($U_1$), narrowed exploration ($U_2$), expanded exploitation ($U_3$) and narrowed exploitation ($U_4$). In ($U_1$), the best hunting area is recognized with high soar and vertical stoop on which AO explores the search space as shown in Eq. (3).

$$U_1(it+1) = U_{best}(it) \times \left(1 - \frac{it}{Tmax}\right) + (U_M(it) - U_{best}(it) * rand) \tag{3}$$

here $U_1(it+1)$, $U_{best}(it)$ and $\left(1 - \frac{it}{Tmax}\right)$ are solution for next iteration, best solution, and search space control parameter, respectively. $U_M(it)$ is the mean value as shown in Eq. (4).

$$U_M(it) = \frac{1}{p_s} \sum_{i=1}^{p_s} U_i(it), \forall j = 1, 2 \ldots Dim \tag{4}$$

In ($U_2$), the Aquila circles around the target, prepares the land and attack after finding the prey. It uses contour fight with a short glide attack and the AO uses a narrowly explored target area as shown in Eq. (5).

$$U_2(it+1) = U_{best}(it) \times levy(Dim) + U_R(it) - (y - u) * rand \tag{5}$$

here $U_2(it+1)$, and $U_R(it)$ are next solution and random solution, respectively. The levy(Dim) is the distribution function is shown in Eq. (6).

$$levy(Dim) = v \times \frac{\delta \times \sigma}{|d|^{\frac{1}{\alpha}}} \tag{6}$$

here v, α, δ, and d are 0.01, 1.5 and random numbers, respectively. σ is shown in Eq. (7).

$$\sigma = \left( \frac{\Gamma(1+\alpha) \times \sin\left(\frac{\pi\alpha}{2}\right)}{\Gamma\left(\frac{1+\alpha}{2}\right) \times \alpha \times 2^{\left(\frac{\alpha-1}{2}\right)}} \right) \tag{7}$$

y and u represents spiral search as shown in Eqs. (8) and (9).

$$y = h \times \cos(\varphi) \tag{8}$$

$$u = h \times \sin(\varphi) \tag{9}$$

h and φ are shown in Eqs. (10) and (11).

$$h = h_1 + W \times Dim_1 \tag{10}$$

$$\varphi = -\epsilon \times Dim_1 + \varphi_1 \tag{11}$$

$\varphi_1$ is shown in Eq. (12).

$$\varphi_1 = \frac{3\pi}{2} \tag{12}$$

where W, ϵ and h are fixed to 0.00565, 0.005 and 1–20, respectively. In $U_3$, the area of prey is accurately described, the Aquila is set for landing and attack, for which it uses low-flight with slow descent attack for discovering prey reaction as shown in Eq. (13).

$$U_3(it+1) = (U_{best}(it) - U_M(it)) \times \varepsilon - rand + ((Ub - Lb) \times rand + Lb) \times \beta \tag{13}$$

where $U_3(it+1)$, $\varepsilon$, $\beta$, $U_{best}(it)$ and $U_M(it)$ are the next iteration solution, exploitation adjustment factors, best solution, and mean solution, respectively. In $U_4$, the Aquila gets close to prey based on the stochastic movement by using the walk and grab prey method. Then the AO attacks based on the last movement, as shown in Eq. (14).

$$U_4(it+1) = QF \times U_{best}(it) - (P_1 \times U(it) \times rand) - P_2 \times levy(Dim) + rand \times P_1 \tag{14}$$

$U_4(it+1)$ is the next solution. Quality factor (QF), variation of motion $P_1$ and $P_2$ are shown in Eqs. (15)–(17), respectively.

$$QF(it) = it^{\frac{2\times rand-1}{(1-Tmax)^2}} \tag{15}$$

$$P_1 = 2 \times rand - 1 \tag{16}$$

$$P_2 = 2 \times \left(1 - \frac{it}{Tmax}\right) \tag{17}$$

The pseudo code implementation of AO is shown in Algorithm 1.

**Algorithm 1:** AO pseudo code

```
Initialize U, ε, and β.
while do
Calculate fitness.
Determine U_best.
    for j = 1: p_s
    Update U_M(it).
    Update u, y, P_1, P_2 and levy(Dim).
        if it ≤ (2/3) * Tmax
            if rand ≤ 0.5
              Update U_1(it+1) using (3).
              if (fitness U_1(it+1) < fitness U(it))
                 U(it) = U_1(it+1)
              if (fitness U_1(it+1) < fitness U_best(it))
                 U_best(it) = U_1(it+1)
              end
              end
            else
              Update U_2(it+1) using (5).
              if (fitness U_2(it+1) < fitness U(it))
                  U(it) = U_2(it+1)
              if (fitness U_2(it+1) < fitness U_best(it))
                  U_best(it) = U_2(it+1)
```

(Continued)

**Algorithm 1 (continued)**

```
            end
            end
            end
          else if rand ≤ 0.5
            Update U3(it + 1) using (13).
           if (fitness U3(it + 1) < fitness U(it))
               U(it) = U3(it + 1)
           if (fitness U3(it + 1) < fitness Ubest(it))
               Ubest(it) = U3(it + 1)
           end
           end
          else
            Update U4(it + 1) using (14).
           if (fitness U4(it + 1) < fitness U(it))
              U(it) = U4(it + 1)
           if (fitness U4(it + 1) < fitness Ubest(it))
              Ubest(it) = U4(it + 1)
           end
           end
           end
           end
        end
    end
    return Ubest
```

### *2.2 Chaotic Aquila Optimizer (CAO)*

Chaotic maps are integrated into OT to maximize its exploration and exploitation capabilities. These maps generate ergodic values used in OT for escaping the local minima. Moreover, they dynamically manage the smooth transitions between local and global search, which accelerates the convergence and maintains population diversity. In this work, the narrowed exploitation mechanism of AO is improved by integrating ten well-known chaotic maps into the QF of AO. These maps use chaotic values to balance the exploration and exploitation of AO and modulate transition timing based on search diversity. CAO is first tested on twenty-three mathematical and ten CEC benchmark functions having both unimodal and multimodal features, followed by a parameter estimation of EHCS. A brief comparison between AO and CAO is summarized in Table 3.

These details of these maps were given in Table 4.

These chaotic maps ($C_m$) are integrated in QF of AO. Eq. (15) is updated for CAO as shown in Eq. (18).

$$QF_C(it) = it^{\frac{2\times C_m - 1}{(1-Tmax)^2}} \tag{18}$$

$U_4(it+1)$ is shown in Eq. (19).

$$U_4(it+1) = QF_C \times U_{best}(it) - (P_1 \times U(it) \times rand) - P_2 \times levy(Dim) + rand \times P_1 \tag{19}$$

**Table 3:** Comparison between AO and CAO

| AO | CAO |
|---|---|
| Slow convergence | Fast convergence |
| Low solution quality | High solution quality |
| Low local minima avoidance | High local minima avoidance |
| Low scalability | Scalable on higher dimension problems |

**Table 4:** Chaotic maps

| OT | Chaotic maps and relations | |
|---|---|---|
| CAO1 | Chebyshev map [74] | $x_{w+1} = \cos\left(w \cos^{-1}\left(x_w\right)\right)$ |
| CAO2 | Circle map [75] | $x_{w+1} = \mathrm{mod}\left(x_w + 0.2 - \left(\frac{0.5}{2\pi}\right)\sin\left(2\pi x_w\right), 1\right)$ |
| CAO3 | Gauss/mouse map [76] | $x_{w+1} = \begin{cases} 1, x_w = 0 \\ \frac{1}{\mathrm{mod}\left(x_w, 1\right)} \end{cases}$ otherwise |
| CAO4 | Iterative map [77] | $x_{w+1} = \sin\left(\frac{0.7\pi}{x_w}\right)$ |
| CAO5 | Logistic map [78] | $x_{w+1} = 4x_w\left(1 - x_w\right)$ |
| CAO6 | Piecewise map [79] | $x_{w+1} = \begin{cases} \frac{x_w}{0.4}, 0 \le x_w < 0.4 \\ \frac{x_w - 0.4}{0.1}, 0.4 \le x_w < 0.5 \\ \frac{0.6 - x_w}{0.1}, 0.5 \le x_w < 0.6 \\ \frac{1 - x_w}{0.4}, 0.6 \le x_w < 1 \end{cases}$ |
| CAO7 | Sine map [80] | $x_{w+1} = \sin\left(\pi x_w\right)$ |
| CAO8 | Singer map [81] | $x_{w+1} = 1.07\left(7.86x_w - 23.31x_w^2 + 28.75x_w^3 - 13.30x_w^4\right)$ |
| CAO9 | Sinusoidal map [82] | $x_{w+1} = 2.3x_w^2 \sin\left(\pi x_w\right)$ |
| CAO10 | Tent map [83] | $x_{w+1} = \begin{cases} \frac{x_w}{0.7}, x_w < 0.7 \\ 10/3\left(1 - x_w\right), x_w \ge 0.7 \end{cases}$ |

The pseudo code implementation of CAO is shown in Algorithm 2.

**Algorithm 2:** CAO pseudo code

Initialize $U$, $\varepsilon$, and $\beta$.
while do
Calculate fitness.
Determine $U_{best}$.
for $j = 1: p_s$
Update $U_M(it)$.
Update $u, y, P_1, P_2$ and $levy(Dim)$.
if $it \leq (2/3) * Tmax$
if rand $\leq 0.5$
Update $U_1(it+1)$ using (3).
if (fitness $U_1(it+1) <$ fitness $U(it)$)
$U(it) = U_1(it+1)$
if (fitness $U_1(it+1) <$ fitness $U_{best}(it)$)
$U_{best}(it) = U_1(it+1)$
end
end
else
Update $U_2(it+1)$ using (5).
if (fitness $U_2(it+1) <$ fitness $U(it)$)
$U(it) = U_2(it+1)$
if (fitness $U_2(it+1) <$ fitness $U_{best}(it)$)
$U_{best}(it) = U_2(it+1)$
end
end
end
else if rand $\leq 0.5$
Update $U_3(it+1)$ using (13).
if (fitness $U_3(it+1) <$ fitness $U(it)$)
$U(it) = U_3(it+1)$
if (fitness $U_3(it+1) <$ fitness $U_{best}(it)$)
$U_{best}(it) = U_3(it+1)$
end
end
else
Update $U_4(it+1)$ using (19).
if (fitness $U_4(it+1) <$ fitness $U(it)$)
$U(it) = U_4(it+1)$
if (fitness $U_4(it+1) <$ fitness $U_{best}(it)$)
$U_{best}(it) = U_4(it+1)$
end
end
end
end

(Continued)

**Algorithm 2 (continued)**

```
    end
  end
  return U_best
```

### *2.3 Fitness Evaluation*

CAO is assessed by using the fitness evaluation as shown in Eq. (20).

$$FE = \text{mean}\left(\varphi - \hat{\varphi}\right)^2 \tag{20}$$

where $\varphi$ and $\hat{\varphi}$ are the desired and estimated responses.

## 3 Performance Analyses

This section provides the analysis of AO and its chaotic variants for mathematical benchmark and CEC functions.

### *3.1 Mathematical Functions Analysis*

On 100 independent executions, the investigation for mathematical benchmark functions at $p_s$ = 50, and Tmax = 1000 is conducted, which is shown in Tables 5 and 6. In Tables 5 and 6, CAO9, CAO6, CAO9, CAO5, CAO4, AO, CAO3, AO, CAO6, CAO3, CAO9, CAO2, CAO2, CAO2, CAO2, CAO2 and CAO1 have better performance for F1, F2, F3, F4, F5, F7, F8, F12, F13, F14, F15, F16, F17, F18, F19, F20 and F23 functions, respectively. In functions F6, F9, F10, F11, F21, and F22, all methods have similar performance.

**Table 5:** Average fitness analysis of AO, CAO1, CAO2, CAO3, CAO4 and CAO5 on benchmark functions

| Functions | AO | CAO1 | CAO2 | CAO3 | CAO4 | CAO5 |
|---|---|---|---|---|---|---|
| F1 | 4.873E−211 | 4.178E−201 | 8.098E−210 | 1.938E−207 | 1.797E−218 | 6.032E−204 |
| F2 | 1.581E−126 | 1.009E−117 | 5.416E−105 | 2.222E−108 | 6.901E−108 | 4.860E−124 |
| F3 | 1.255E−203 | 3.450E−206 | 1.134E−201 | 4.791E−209 | 2.392E−204 | 4.285E−206 |
| F4 | 2.233E−107 | 5.791E−106 | 2.560E−104 | 7.776E−105 | 2.683E−107 | 6.432E−109 |
| F5 | 4.738E−04 | 6.083E−04 | 5.454E−04 | 3.586E−04 | 2.713E−04 | 3.629E−04 |
| F6 | 0 | 0 | 0 | 0 | 0 | 0 |
| F7 | 2.907E−05 | 3.519E−05 | 3.379E−05 | 3.134E−05 | 3.429E−05 | 3.340E−05 |
| F8 | −9.621E+03 | −8.736E+03 | −9.488E+03 | −9.989E+03 | −9.279E+03 | −9.768E+03 |
| F9 | 0 | 0 | 0 | 0 | 0 | 0 |
| F10 | 8.882E−16 | 8.882E−16 | 8.882E−16 | 8.882E−16 | 8.882E−16 | 9.237E−16 |
| F11 | 0 | 0 | 0 | 0 | 0 | 0 |
| F12 | 2.422E−07 | 3.026E−07 | 3.427E−07 | 3.545E−07 | 3.087E−07 | 2.802E−07 |
| F13 | 2.928E−06 | 2.553E−06 | 3.077E−06 | 2.503E−06 | 2.590E−06 | 2.224E−06 |
| F14 | 1.548E+00 | 1.382E+00 | 1.254E+00 | 1.227E+00 | 1.334E+00 | 1.852E+00 |
| F15 | 4.185E−04 | 4.295E−04 | 4.030E−04 | 4.527E−04 | 4.154E−04 | 4.071E−04 |
| F16 | −1.032 | −1.031 | −1.032 | −1.031 | −1.031 | −1.031 |
| F17 | 3.979E−01 | 3.980E−01 | 3.979E−01 | 3.981E−01 | 3.980E−01 | 3.980E−01 |
| F18 | 3.009 | 3.018 | 3.006 | 3.035 | 3.016 | 3.015 |
| F19 | −3.860 | −3.858 | −3.861 | −3.855 | −3.860 | −3.859 |

(Continued)

**Table 5 (continued)**

| Functions | AO | CAO1 | CAO2 | CAO3 | CAO4 | CAO5 |
|---|---|---|---|---|---|---|
| F20 | −3.206 | −3.196 | −3.232 | −3.134 | −3.213 | −3.188 |
| F21 | −1.015E+01 | −1.015E+01 | −1.015E+01 | −1.015E+01 | −1.015E+01 | −1.015E+01 |
| F22 | −1.040E+01 | −1.040E+01 | −1.040E+01 | −1.040E+01 | −1.040E+01 | −1.040E+01 |
| F23 | −1.053E+01 | −1.054E+01 | −1.054E+01 | −1.053E+01 | −1.053E+01 | −1.053E+01 |

**Table 6:** Average fitness analysis of AO, CAO6, CAO7, CAO8, CAO9 and CAO10 on benchmark functions

| Functions | AO | CAO6 | CAO7 | CAO8 | CAO9 | CAO10 |
|---|---|---|---|---|---|---|
| F1 | 4.873E−211 | 5.491E−211 | 5.873E−222 | 7.542E−210 | 6.430E−223 | 1.138E−212 |
| F2 | 1.581E−126 | 1.397E−145 | 2.791E−113 | 1.165E−142 | 7.273E−105 | 3.823E−121 |
| F3 | 1.255E−203 | 4.160E−203 | 4.644E−202 | 4.064E−205 | 3.178E−209 | 4.734E−206 |
| F4 | 2.233E−107 | 3.307E−104 | 5.931E−104 | 1.198E−106 | 7.289E−106 | 1.266E−107 |
| F5 | 4.738E−04 | 4.774E−04 | 3.508E−04 | 4.660E−04 | 5.512E−04 | 3.991E−04 |
| F6 | 0 | 0 | 0 | 0 | 0 | 0 |
| F7 | 2.907E−05 | 3.637E−05 | 3.560E−05 | 3.606E−05 | 3.485E−05 | 3.800E−05 |
| F8 | −9.621E+03 | −9.749E+03 | −9.292E+03 | −9.261E+03 | −9.110E+03 | −9.498E+03 |
| F9 | 0 | 0 | 0 | 0 | 0 | 0 |
| F10 | 8.882E−16 | 8.882E−16 | 8.882E−16 | 8.882E−16 | 8.882E−16 | 8.882E−16 |
| F11 | 0 | 0 | 0 | 0 | 0 | 0 |
| F12 | 2.422E−07 | 2.829E−07 | 2.909E−07 | 3.353E−07 | 2.765E−07 | 3.321E−07 |
| F13 | 2.928E−06 | 1.936E−06 | 2.652E−06 | 3.119E−06 | 2.989E−06 | 2.776E−06 |
| F14 | 1.548E+00 | 1.539E+00 | 1.334E+00 | 1.569E+00 | 1.665E+00 | 1.382E+00 |
| F15 | 4.185E−04 | 4.118E−04 | 4.105E−04 | 4.000E−04 | 3.971E−04 | 4.002E−04 |
| F16 | −1.032 | −1.03 | −1.031 | −1.031 | −1.032 | −1.032 |
| F17 | 3.979E−01 | 3.980E−01 | 3.980E−01 | 3.980E−01 | 3.980E−01 | 3.980E−01 |
| F18 | 3.009 | 3.008 | 3.010 | 3.013 | 3.011 | 3.011 |
| F19 | −3.860 | −3.860 | −3.859 | −3.860 | −3.860 | −3.861 |
| F20 | −3.206 | −3.225 | −3.194 | −3.200 | −3.190 | −3.224 |
| F21 | −1.015E+01 | −1.015E+01 | −1.015E+01 | −1.015E+01 | −1.015E+01 | −1.015E+01 |
| F22 | −1.040E+01 | −1.040E+01 | −1.040E+01 | −1.040E+01 | −1.040E+01 | −1.040E+01 |
| F23 | −1.053E+01 | −1.054E+01 | −1.054E+01 | −1.053E+01 | −1.053E+01 | −1.053E+01 |

The convergence analysis of AO and CAO1-10 for mathematical functions is shown in Figs. 1–4 where legend is provided in Fig. 4. Fig. 1a–f shows the convergence for F1, F2, F3, F4, F5 and F6 functions. Similarly, Figs. 2a–f, 3a–f and 4a–e show the convergence for F7, F8, F9, F10, F11, F12, F13, F14, F15, F16, F17, F18, F19, F20, F21, F22, and F23 functions, respectively. It is depicted from Figs. 1–4 that chaotic variants of AO show better convergence for these functions than AO.

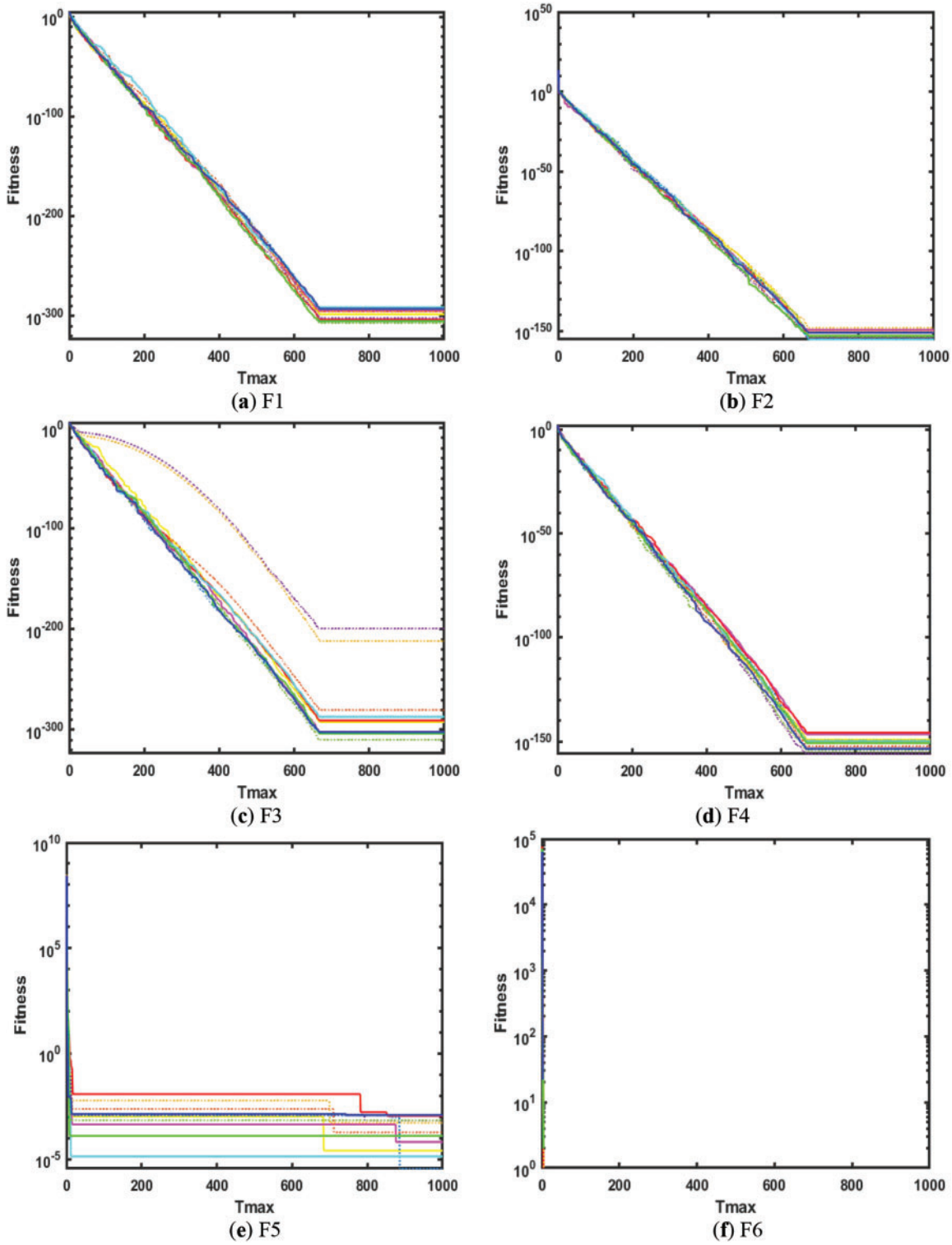


**Figure 1:** Convergence analysis on F1, F2, F3, F4, F5 and F6 mathematical functions

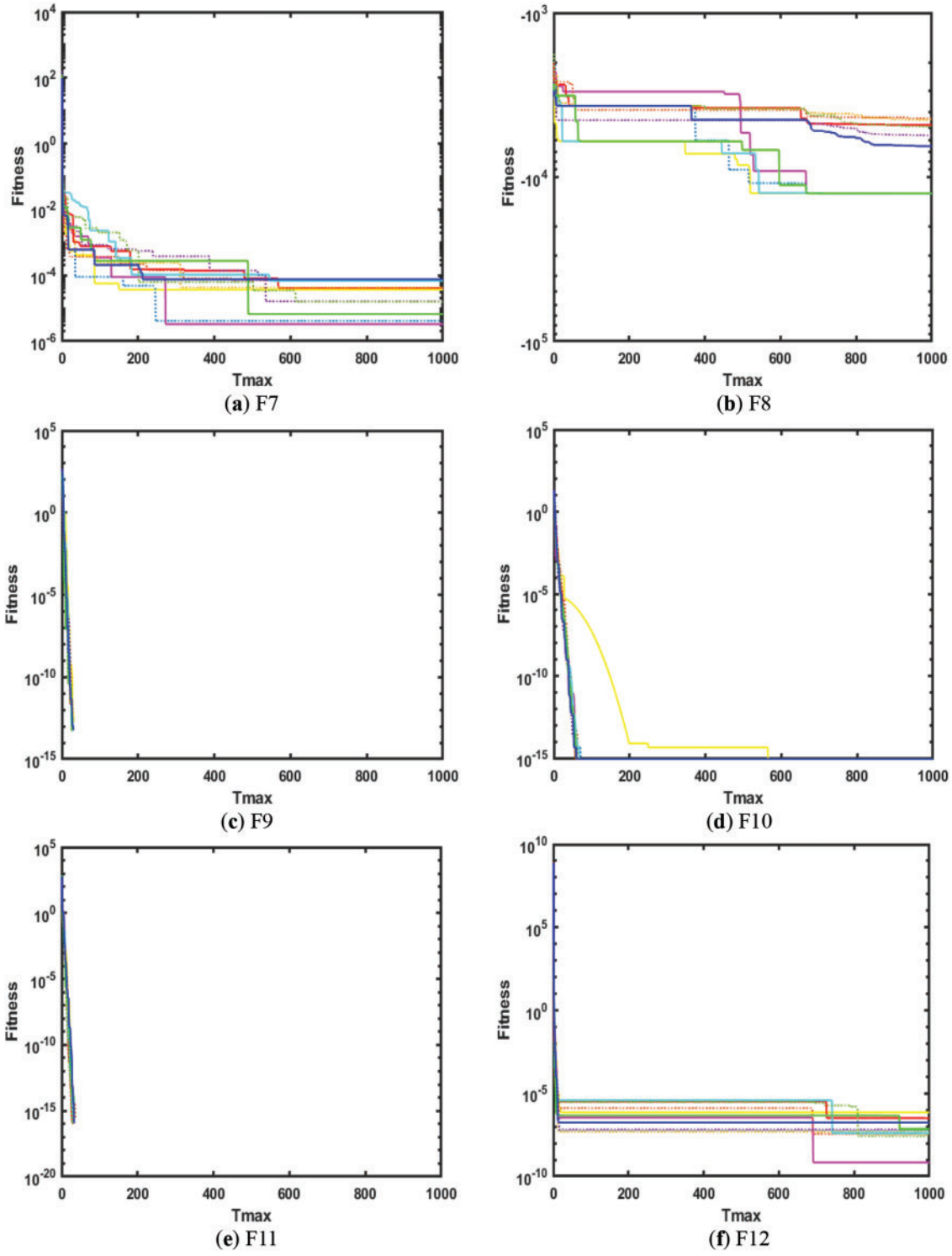


**Figure 2:** Convergence analysis on F7, F8, F9, F10, F11 and F12 mathematical functions

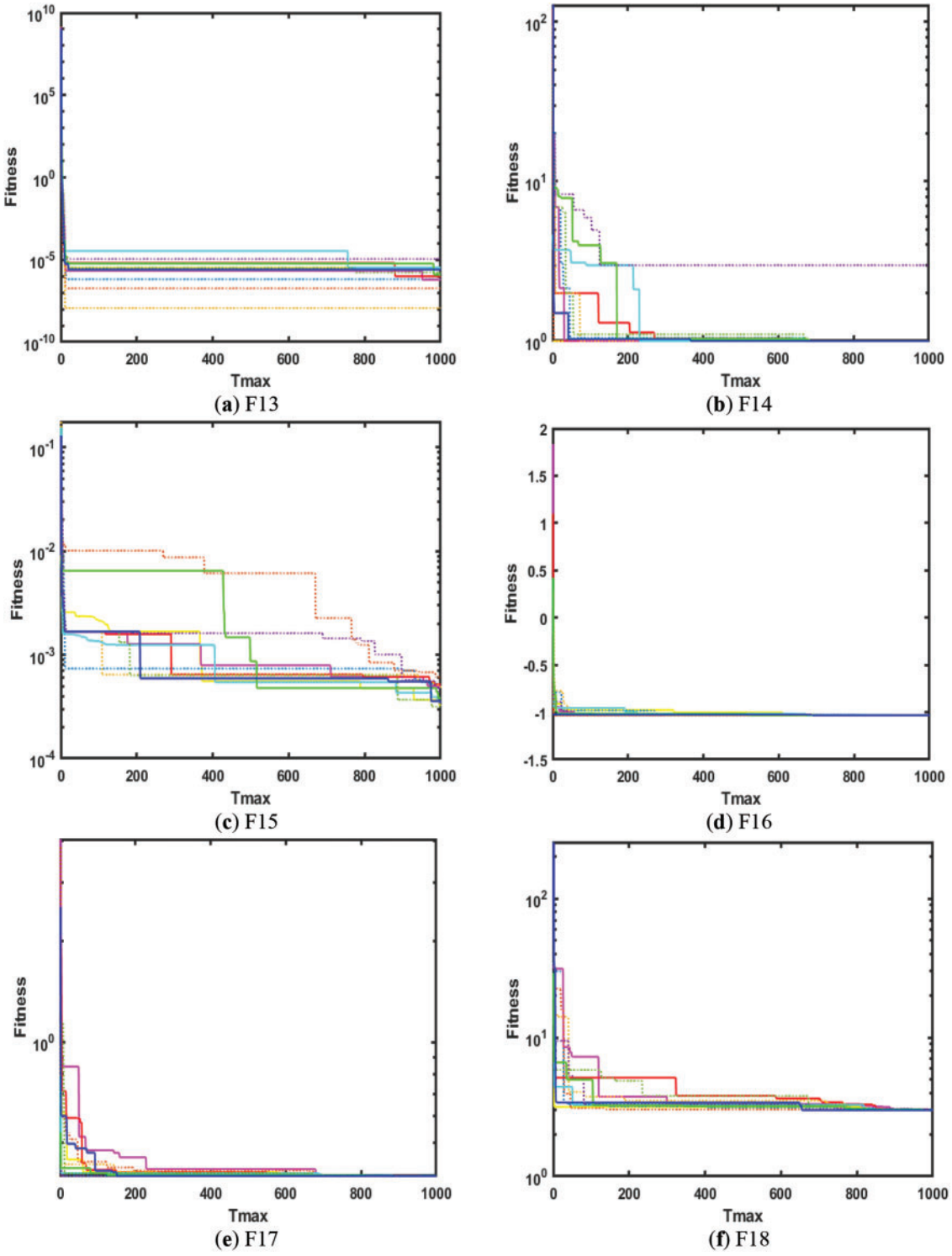


**Figure 3:** Convergence analysis on F13, F14, F15, F16, F17 and F18 mathematical functions

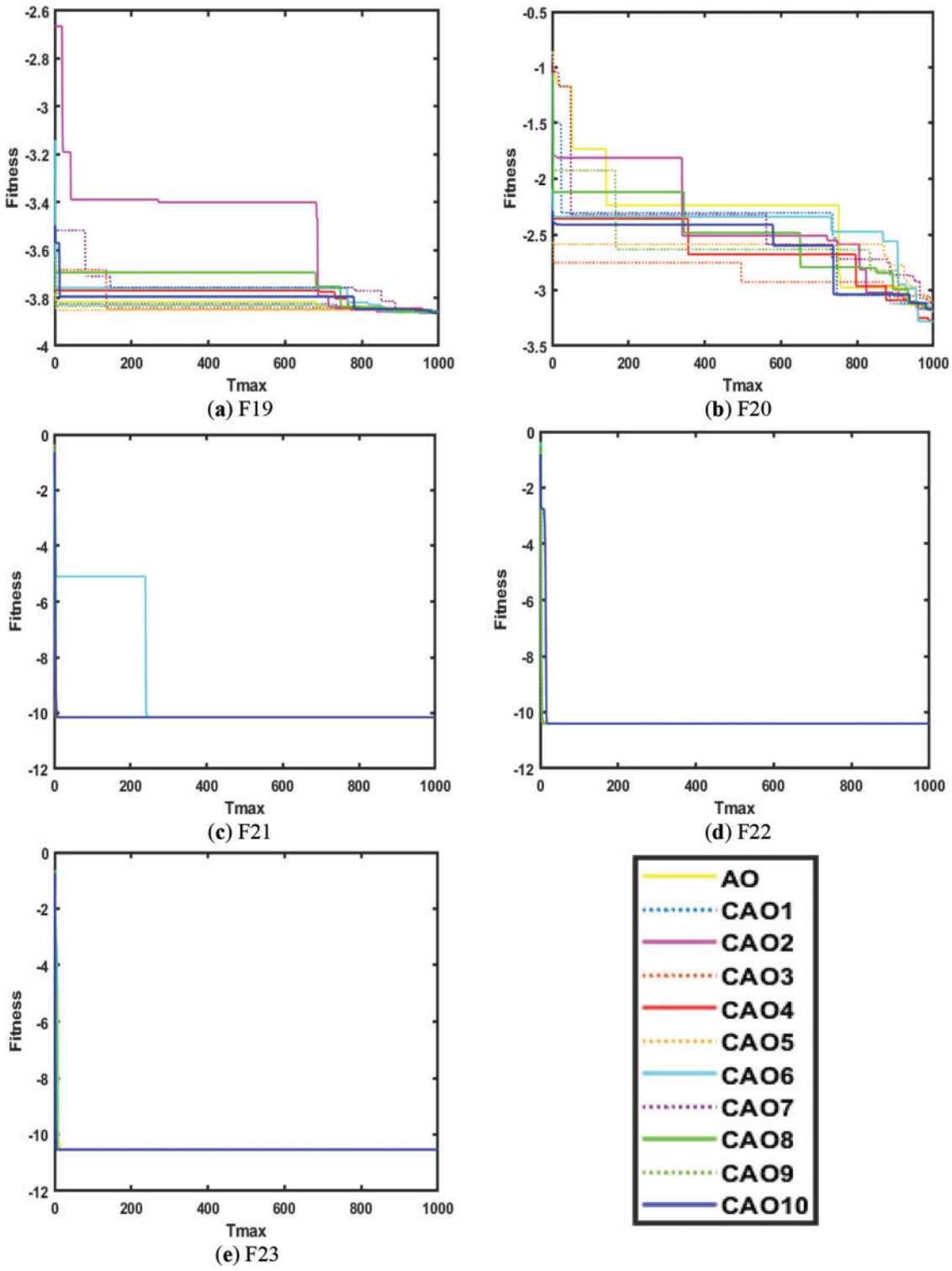


**Figure 4:** Convergence analysis on F19, F20, F21, F22 and F23 mathematical functions

### *3.2 CEC Functions Analysis*

On 100 independent executions, the investigation for the CEC2019 benchmark functions at $p_s$ = 50, and Tmax = 1000 is conducted, which is shown in Tables 7 and 8. In Tables 7 and 8, CAO2, CAO5, AO, CAO2, CAO2, CAO6, CAO10, CAO2, and CAO6 have better performance for CEC1 to CEC10 functions, respectively. In CEC3, all techniques have similar performance.

**Table 7:** Average fitness analysis of AO, CAO1, CAO2, CAO3, CAO4 and CAO5 on CEC2019 functions

| Functions | AO | CAO1 | CAO2 | CAO3 | CAO4 | CAO5 |
|---|---|---|---|---|---|---|
| CEC1 | 4.831E+04 | 4.964E+04 | 4.757E+04 | 5.996E+04 | 4.940E+04 | 4.910E+04 |
| CEC2 | 1.736E+01 | 1.737E+01 | 1.736E+01 | 1.740E+01 | 1.737E+01 | 1.736E+01 |
| CEC3 | 1.270E+01 | 1.270E+01 | 1.270E+01 | 1.270E+01 | 1.270E+01 | 1.270E+01 |
| CEC4 | 1.549E+02 | 2.251E+02 | 1.610E+02 | 1.008E+03 | 1.938E+02 | 1.892E+02 |
| CEC5 | 1.326E+00 | 1.382E+00 | 1.309E+00 | 1.925E+00 | 1.349E+00 | 1.380E+00 |
| CEC6 | 9.911E+00 | 1.027E+01 | 9.761E+00 | 1.038E+01 | 1.024E+01 | 1.025E+01 |
| CEC7 | 2.923E+02 | 3.264E+02 | 2.844E+02 | 4.378E+02 | 3.045E+02 | 2.884E+02 |
| CEC8 | 4.855E+00 | 5.053E+00 | 4.762E+00 | 5.302E+00 | 4.907E+00 | 4.780E+00 |
| CEC9 | 3.639E+00 | 4.227E+00 | 3.493E+00 | 3.202E+01 | 3.958E+00 | 3.960E+00 |
| CEC10 | 1.755E+01 | 1.725E+01 | 1.609E+01 | 1.961E+01 | 1.625E+01 | 1.711E+01 |

**Table 8:** Average fitness analysis of AO, CAO6, CAO7, CAO8, CAO9 and CAO10 on CEC2017 functions

| Functions | AO | CAO6 | CAO7 | CAO8 | CAO9 | CAO10 |
|---|---|---|---|---|---|---|
| CEC1 | 4.831E+04 | 4.803E+04 | 5.004E+04 | 4.874E+04 | 4.902E+04 | 4.917E+04 |
| CEC2 | 1.736E+01 | 1.736E+01 | 1.736E+01 | 1.736E+01 | 1.736E+01 | 1.736E+01 |
| CEC3 | 1.270E+01 | 1.270E+01 | 1.270E+01 | 1.270E+01 | 1.270E+01 | 1.270E+01 |
| CEC4 | 1.549E+02 | 1.765E+02 | 1.919E+02 | 2.422E+02 | 2.760E+02 | 1.632E+02 |
| CEC5 | 1.326E+00 | 1.370E+00 | 1.384E+00 | 1.380E+00 | 1.429E+00 | 1.330E+00 |
| CEC6 | 9.911E+00 | 9.804E+00 | 9.808E+00 | 1.002E+01 | 9.986E+00 | 9.885E+00 |
| CEC7 | 2.923E+02 | 2.643E+02 | 2.836E+02 | 2.877E+02 | 2.791E+02 | 2.977E+02 |
| CEC8 | 4.855E+00 | 4.821E+00 | 4.845E+00 | 4.905E+00 | 4.850E+00 | 4.738E+00 |
| CEC9 | 3.639E+00 | 3.572E+00 | 3.996E+00 | 3.900E+00 | 3.497E+00 | 3.772E+00 |
| CEC10 | 1.755E+01 | 1.603E+01 | 1.631E+01 | 1.696E+01 | 1.790E+01 | 1.671E+01 |

The convergence analysis of AO and CAO1-10 for CEC functions is shown in Figs. 5 and 6. Fig. 5a–e shows the convergence for CEC1, CEC2, CEC3, CEC4, and CEC5 functions, whereas Fig. 6a–e shows the convergence of CEC6, CEC7, CEC8, CEC9, and CEC10 functions, respectively. It is observed from Figs. 5 and 6 that chaotic variants of AO show better convergence for these functions than AO.

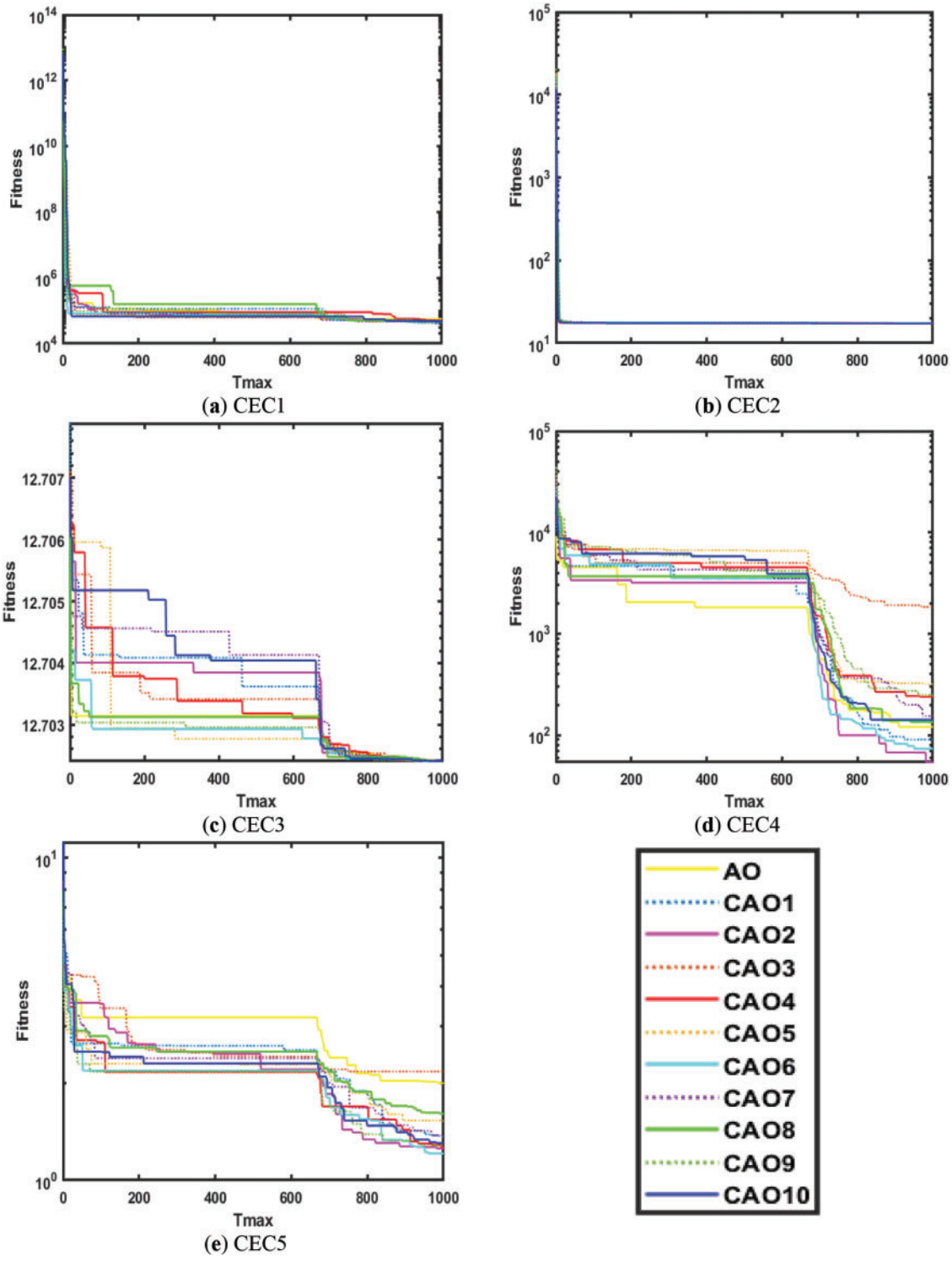


**Figure 5:** Convergence analysis on CEC1, CEC2, CEC3, CEC4 and CEC5 functions

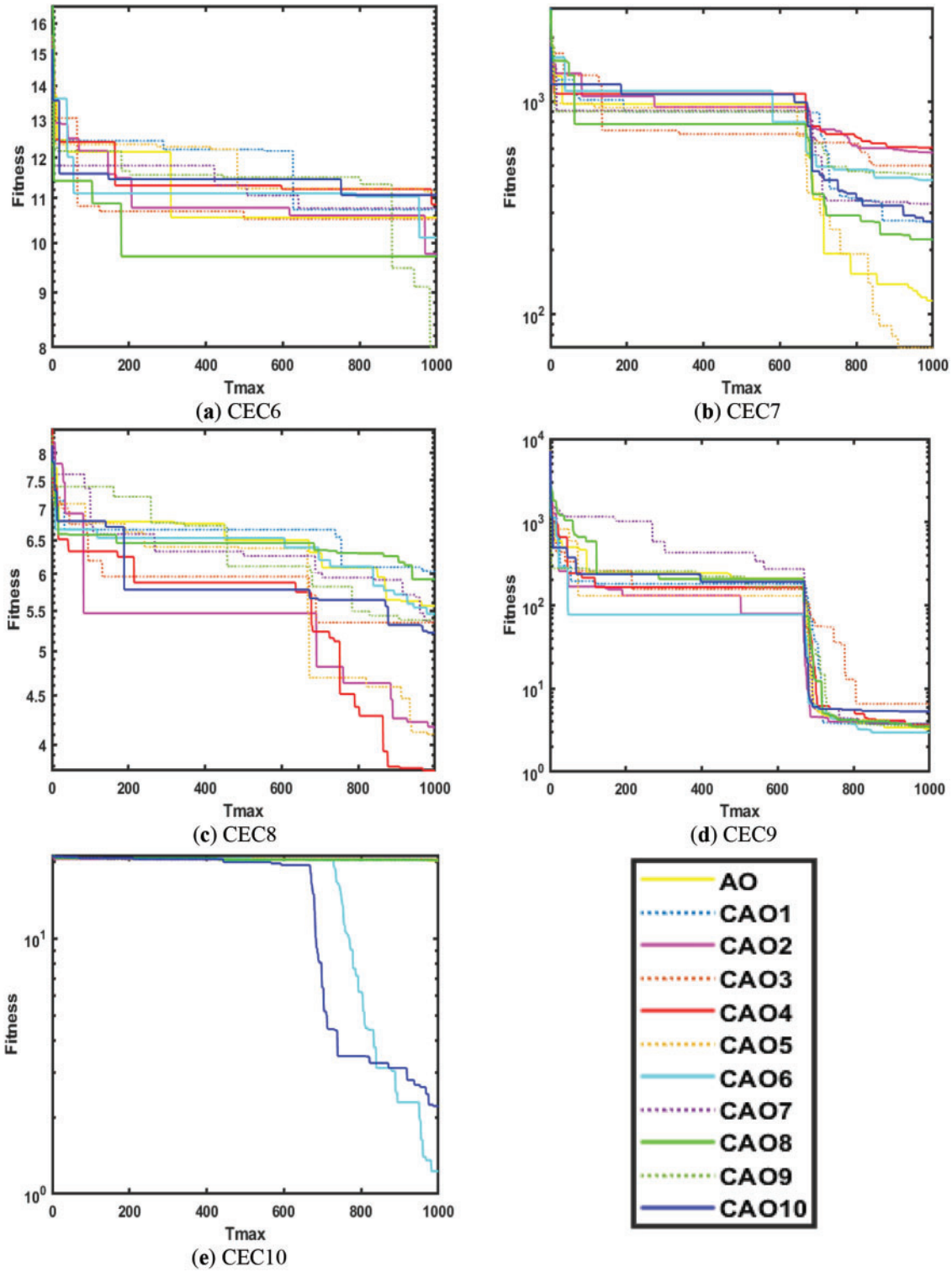


**Figure 6:** Convergence analysis on CEC6, CEC7, CEC8, CEC9 and CEC10 functions

## 4 EHCS Analysis

The electro-hydraulic control system (EHCS) has been recently used in various applications [84]. It consists of an EH proportional valve and a valve-controlled asymmetric subsystem. It can be presented as a first-order model as shown in Eq. (21).

$$\tau_v \dot{d}_v + d_v = g_v \, \epsilon_v \tag{21}$$

where $\tau_v, d_v, g_v$ and $\epsilon_v$ are the time constant, main valve displacement, gain of the EH proportional valve, and effective input, respectively. Its mathematical model is shown in Eqs. (22)–(24).

$$A(d)\, y(t) = B(d)\, \delta(t) + \rho(t) \tag{22}$$

$$A(d) = 1 + a_1 d^{-1} + a_2 d^{-2} + \ldots + a_n d^{-n} \tag{23}$$

$$B(d) = b_0 + b_1 d^{-1} + b_2 d^{-2} + \ldots + b_{n-1} d^{1-n} \tag{24}$$

where $A(d), B(d), \delta(t), \rho(t)$ and $y(t)$ are polynomials, input, noise, and output, respectively. The actual parameters of the EHCS model are taken from [85] as shown in Eqs. (25) and (26).

$$A(d) = 1 - 0.0276 d^{-1} + 0.0124 d^{-2} + 0.0514 d^{-3} \tag{25}$$

$$B(d) = -0.0661 d^{-1} - 0.0653 d^{-2} - 0.0619 d^{-3} \tag{26}$$

the simulations were performed at $p_s$ = 12, 50, Tmax = 1000 and $\rho(t)$ = [1.300E−01, 1.300E−02, 1.300E−03] for hundred independent runs. The tuned parameters of AO, AOA, CAO1-10, RSA, and WOA are given in Table 9.

**Table 9:** Tuned parameter settings of OT

| OT | Tuned parameters |
|---|---|
| AO | Alpha = 0.1, Delta = 0.1, [45] |
| CAO1-10 | $C_{init}$ = 0.7, Alpha = 0.1, Delta = 0.1 |
| AOA | Alpha = 5, beta = 0.5, [68] |
| RSA | Alpha = 0.1, Beta = 0.1, [82] |
| WOA | Alpha = [2 0], [74] |

Tables 10–12 reflect the behavior of AO, CAO1-10, AOA, RSA, and WOA for true values, and best fitness ($f_b$) values for $p_s$ = 12, 50, Tmax = 1000 and $\rho(t)$ = [1.300E−01, 1.300E−02, 1.300E−03]. It is projected that for all variations, noise CAO1-10 attains the finest values against AO, AOA, RSA, and WOA.

**Table 10:** EHCS analysis w.r.t 1.300E−03 noise level

| OT | $p_s$ | $a_1$ | $a_2$ | $a_3$ | $b_1$ | $b_2$ | $b_3$ | $f_b$ |
|---|---|---|---|---|---|---|---|---|
| AOA | 12 | 0.00000 | 0.00000 | 0.00000 | 0.00000 | 0.00000 | −0.19018 | 1.667E−03 |
| | 50 | −0.71457 | 0.00000 | 0.35307 | −0.11601 | 0.00000 | 0.00000 | 1.517E−03 |
| AO | 12 | −0.04011 | 0.05148 | −0.01836 | −0.06433 | −0.07720 | −0.04888 | 8.438E−05 |
| | 50 | −0.07321 | 0.10067 | 0.00066 | −0.06600 | −0.05958 | −0.06618 | 1.322E−05 |
| CAO1 | 12 | −0.05361 | 0.00786 | −0.00307 | −0.05778 | −0.06865 | −0.05367 | 6.205E−05 |

(Continued)

**Table 10 (continued)**

| OT | $p_s$ | $a_1$ | $a_2$ | $a_3$ | $b_1$ | $b_2$ | $b_3$ | $f_b$ |
|---|---|---|---|---|---|---|---|---|
| | 50 | −0.03362 | 0.12790 | −0.01143 | −0.06114 | −0.06363 | −0.07265 | 6.530E−05 |
| CAO2 | 12 | −0.05782 | −0.05140 | 0.13430 | −0.06995 | −0.06267 | −0.05713 | 3.082E−05 |
| | 50 | −0.01636 | 0.03297 | 0.04973 | −0.06141 | −0.06034 | −0.07586 | 1.889E−05 |
| CAO3 | 12 | 0.01934 | 0.01444 | 0.00382 | −0.05535 | −0.06983 | −0.06888 | 3.094E−05 |
| | 50 | −0.03119 | 0.03920 | 0.01431 | −0.07930 | −0.06511 | −0.04720 | 2.583E−05 |
| CAO4 | 12 | −0.05452 | 0.04560 | 0.01792 | −0.06843 | −0.07715 | −0.04485 | 5.203E−05 |
| | 50 | −0.01723 | 0.01645 | 0.01380 | −0.06624 | −0.06124 | −0.06324 | 1.355E−05 |
| CAO5 | 12 | 0.04195 | 0.02527 | 0.07255 | −0.06228 | −0.08011 | −0.06755 | 4.415E−05 |
| | 50 | 0.01205 | 0.01670 | 0.02788 | −0.06615 | −0.07814 | −0.05357 | 2.420E−05 |
| CAO6 | 12 | −0.13256 | 0.03020 | 0.03418 | −0.06050 | −0.05624 | −0.05602 | 5.012E−05 |
| | 50 | 0.04122 | 0.01975 | 0.05978 | −0.06938 | −0.07720 | −0.06288 | 2.873E−05 |
| CAO7 | 12 | 0.03767 | −0.02628 | 0.02931 | −0.06701 | −0.06168 | −0.06518 | 2.566E−05 |
| | 50 | −0.02124 | −0.05555 | 0.06890 | −0.07899 | −0.06150 | −0.04545 | 3.765E−05 |
| CAO8 | 12 | −0.05874 | −0.06386 | 0.08555 | −0.07424 | −0.06513 | −0.04232 | 4.697E−05 |
| | 50 | −0.04641 | 0.03727 | 0.06360 | −0.07037 | −0.05839 | −0.06600 | 1.318E−05 |
| CAO9 | 12 | −0.02720 | 0.03318 | 0.02999 | −0.05681 | −0.07752 | −0.05855 | 3.290E−05 |
| | 50 | −0.06758 | 0.02297 | 0.07394 | −0.05353 | −0.06900 | −0.06948 | 2.545E−05 |
| CAO10 | 12 | 0.00070 | −0.04038 | 0.02939 | −0.05102 | −0.08394 | −0.05054 | 9.368E−05 |
| | 50 | −0.02810 | 0.01181 | 0.04725 | −0.06713 | −0.06618 | −0.06109 | 7.881E−06 |
| RSA | 12 | −0.01622 | 0.32120 | −0.34106 | −0.10008 | −0.00172 | −0.07625 | 9.153E−04 |
| | 50 | 0.00755 | −0.01454 | 0.00866 | −0.07636 | −0.06570 | −0.04881 | 4.883E−05 |
| WOA | 12 | 0.02919 | −0.01399 | 0.02053 | −0.07681 | −0.06018 | −0.05704 | 3.045E−05 |
| | 50 | 0.01911 | 0.02310 | 0.02644 | −0.07249 | −0.06357 | −0.06335 | 1.158E−05 |
| True values | | −0.0276 | 0.0124 | 0.0514 | −0.0661 | −0.0653 | −0.0619 | 0 |

**Table 11:** EHCS analysis w.r.t 1.300E−02 noise level

| OT | $p_s$ | $a_1$ | $a_2$ | $a_3$ | $b_1$ | $b_2$ | $b_3$ | $f_b$ |
|---|---|---|---|---|---|---|---|---|
| AOA | 12 | 0.00000 | 0.00000 | 0.00000 | −0.18145 | 0.00000 | 0.00000 | 1.505E−03 |
| | 50 | 0.00000 | 0.00000 | 0.00000 | 0.00000 | −0.08054 | −0.11053 | 7.161E−04 |
| AO | 12 | 0.00322 | 0.03233 | −0.01479 | −0.09079 | −0.06054 | −0.04073 | 1.572E−04 |
| | 50 | −0.07711 | 0.10258 | 0.03300 | −0.07049 | −0.05609 | −0.06776 | 9.919E−05 |
| CAO1 | 12 | −0.07756 | 0.14792 | −0.06226 | −0.08048 | −0.05951 | −0.04923 | 1.347E−04 |
| | 50 | 0.04583 | −0.00737 | 0.02875 | −0.07065 | −0.06226 | −0.06561 | 1.303E−04 |
| CAO2 | 12 | −0.07937 | 0.10401 | 0.00562 | −0.06247 | −0.05198 | −0.07900 | 1.299E−04 |
| | 50 | −0.06648 | 0.04774 | 0.05801 | −0.07288 | −0.06972 | −0.05157 | 9.629E−05 |
| CAO3 | 12 | −0.06682 | 0.06030 | 0.05286 | −0.08261 | −0.04782 | −0.05919 | 1.467E−04 |
| | 50 | −0.00196 | 0.02203 | 0.04722 | −0.05864 | −0.06234 | −0.07776 | 1.321E−04 |
| CAO4 | 12 | −0.06579 | 0.11266 | −0.05368 | −0.07480 | −0.05854 | −0.05294 | 1.364E−04 |
| | 50 | −0.01061 | 0.06346 | 0.01990 | −0.06610 | −0.06946 | −0.06149 | 1.126E−04 |
| CAO5 | 12 | −0.08840 | 0.11583 | 0.04073 | −0.06166 | −0.06657 | −0.07231 | 1.174E−04 |

(Continued)

**Table 11 (continued)**

| OT | $p_s$ | $a_1$ | $a_2$ | $a_3$ | $b_1$ | $b_2$ | $b_3$ | $f_b$ |
|---|---|---|---|---|---|---|---|---|
| | 50 | −0.04712 | 0.14242 | −0.01704 | −0.08732 | −0.05409 | −0.05798 | 1.146E−04 |
| CAO6 | 12 | −0.02931 | −0.01474 | 0.07889 | −0.06088 | −0.06295 | −0.06995 | 1.295E−04 |
| | 50 | −0.00015 | 0.04811 | 0.00725 | −0.07469 | −0.06221 | −0.06044 | 1.014E−04 |
| CAO7 | 12 | 0.04689 | 0.04341 | 0.00840 | −0.07860 | −0.06108 | −0.06140 | 1.419E−04 |
| | 50 | −0.04321 | 0.02917 | 0.08693 | −0.06173 | −0.06546 | −0.07040 | 1.127E−04 |
| CAO8 | 12 | −0.03285 | 0.01104 | 0.05955 | −0.06451 | −0.06438 | −0.06287 | 1.094E−04 |
| | 50 | −0.07822 | 0.02420 | 0.10229 | −0.07227 | −0.05404 | −0.06694 | 1.159E−04 |
| CAO9 | 12 | −0.07083 | 0.15143 | −0.07398 | −0.08440 | −0.04899 | −0.05189 | 1.804E−04 |
| | 50 | 0.02229 | 0.11904 | 0.00290 | −0.06710 | −0.07140 | −0.07451 | 1.186E−04 |
| CAO10 | 12 | −0.01898 | 0.09968 | −0.03390 | −0.08921 | −0.05554 | −0.04912 | 1.407E−04 |
| | 50 | −0.08210 | 0.09493 | 0.04378 | −0.08715 | −0.06288 | −0.04677 | 1.023E−04 |
| RSA | 12 | 0.05064 | 0.02501 | −0.01250 | −0.11878 | −0.07952 | −0.00415 | 4.209E−04 |
| | 50 | 0.01163 | −0.00257 | 0.04576 | −0.05385 | −0.10098 | −0.04444 | 2.800E−04 |
| WOA | 12 | −0.02311 | 0.16710 | −0.02802 | −0.06505 | −0.04868 | −0.09360 | 1.886E−04 |
| | 50 | −0.13366 | 0.13252 | −0.00593 | −0.08850 | −0.05207 | −0.04472 | 1.240E−04 |
| True values | | −0.0276 | 0.0124 | 0.0514 | −0.0661 | −0.0653 | −0.0619 | 0 |

**Table 12:** EHCS analysis w.r.t 1.300E−01 noise level

| OT | $p_s$ | $a_1$ | $a_2$ | $a_3$ | $b_1$ | $b_2$ | $b_3$ | $f_b$ |
|---|---|---|---|---|---|---|---|---|
| AOA | 12 | −0.17772 | 0.00000 | 0.00000 | −0.14856 | 0.00000 | 0.00000 | 1.064E−02 |
| | 50 | 0.00000 | 0.00000 | 0.00000 | −0.19106 | 0.00000 | 0.00000 | 1.057E−02 |
| AO | 12 | −0.05015 | 0.15896 | 0.14721 | −0.15149 | −0.07468 | −0.00907 | 8.893E−03 |
| | 50 | −0.05987 | 0.10123 | 0.25712 | −0.14567 | −0.04198 | −0.04565 | 8.722E−03 |
| CAO1 | 12 | −0.01894 | −0.01220 | 0.26858 | −0.13589 | −0.03875 | −0.04967 | 8.920E−03 |
| | 50 | 0.04583 | −0.00737 | 0.02875 | −0.07065 | −0.06226 | −0.06561 | 8.840E−03 |
| CAO2 | 12 | −0.06963 | 0.14822 | 0.20027 | −0.11712 | −0.05590 | −0.05524 | 8.804E−03 |
| | 50 | −0.03384 | 0.11981 | 0.24022 | −0.14374 | −0.05754 | −0.03608 | 8.701E−03 |
| CAO3 | 12 | 0.01743 | 0.09384 | 0.22442 | −0.14914 | −0.02963 | −0.05495 | 8.938E−03 |
| | 50 | −0.00275 | 0.08755 | 0.23777 | −0.14545 | −0.04792 | −0.04457 | 8.713E−03 |
| CAO4 | 12 | 0.03242 | 0.16627 | 0.15411 | −0.12303 | −0.11028 | −0.01199 | 9.115E−03 |
| | 50 | −0.05078 | 0.10988 | 0.22708 | −0.14223 | −0.04605 | −0.03764 | 8.777E−03 |
| CAO5 | 12 | −0.01023 | 0.01537 | 0.16681 | −0.17521 | −0.02844 | −0.01249 | 9.017E−03 |
| | 50 | 0.03109 | 0.12932 | 0.19926 | −0.15685 | −0.06630 | −0.02197 | 8.766E−03 |
| CAO6 | 12 | −0.02293 | 0.07863 | 0.29718 | −0.14582 | −0.05689 | −0.04407 | 8.771E−03 |
| | 50 | −0.04437 | 0.07027 | 0.28387 | −0.15319 | −0.05031 | −0.03229 | 8.728E−03 |
| CAO7 | 12 | −0.08227 | 0.15404 | 0.15671 | −0.17769 | −0.07623 | 0.02925 | 9.088E−03 |
| | 50 | −0.05650 | 0.06065 | 0.28226 | −0.15338 | −0.04095 | −0.03956 | 8.755E−03 |
| CAO8 | 12 | 0.02259 | 0.19302 | 0.14468 | −0.15819 | −0.06091 | −0.02518 | 8.945E−03 |
| | 50 | −0.00250 | 0.07991 | 0.24178 | −0.16990 | −0.05872 | −0.00982 | 8.723E−03 |
| CAO9 | 12 | −0.13119 | 0.09588 | 0.20609 | −0.13292 | −0.05877 | −0.02273 | 8.871E−03 |

(Continued)

**Table 12 (continued)**

| OT | $p_s$ | $a_1$ | $a_2$ | $a_3$ | $b_1$ | $b_2$ | $b_3$ | $f_b$ |
|---|---|---|---|---|---|---|---|---|
| | 50 | −0.10845 | 0.16466 | 0.18827 | −0.12995 | −0.04918 | −0.04497 | 8.786E−03 |
| CAO10 | 12 | −0.07946 | 0.03483 | 0.24237 | −0.12953 | −0.02556 | −0.06259 | 8.946E−03 |
| | 50 | −0.04282 | 0.07211 | 0.24592 | −0.16350 | −0.05025 | −0.01389 | 8.732E−03 |
| RSA | 12 | −0.01424 | 0.00000 | 0.13591 | −0.21132 | 0.00448 | 0.00000 | 9.640E−03 |
| | 50 | −0.00022 | 0.16505 | 0.15488 | −0.09439 | −0.09372 | −0.05188 | 9.083E−03 |
| WOA | 12 | 0.04502 | 0.01181 | 0.26039 | −0.13725 | −0.08115 | −0.02063 | 8.936E−03 |
| | 50 | 0.00046 | 0.11458 | 0.22119 | −0.16439 | −0.04013 | −0.03654 | 8.752E−03 |
| True values | | −0.0276 | 0.0124 | 0.0514 | −0.0661 | −0.0653 | −0.0619 | 0 |

The convergence analysis at $p_s$ = 50, Tmax = 1000 and ρ (t) = [1.300E−01, 1.300E−02, 1.300E−03] of AO, AOA, CAO1-10, RSA, and WOA for EHCS are shown in Figs. 7–9. Fig. 7a–f shows the convergence for AO, and CAO1-5. Similarly, Figs. 8a–f and 9a,b show the convergence for CAO6-10, AOA, RSA, and WOA, respectively. It is observed from Figs. 7–9 that for all OT, with an increase of ρ (t) fitness also increases.

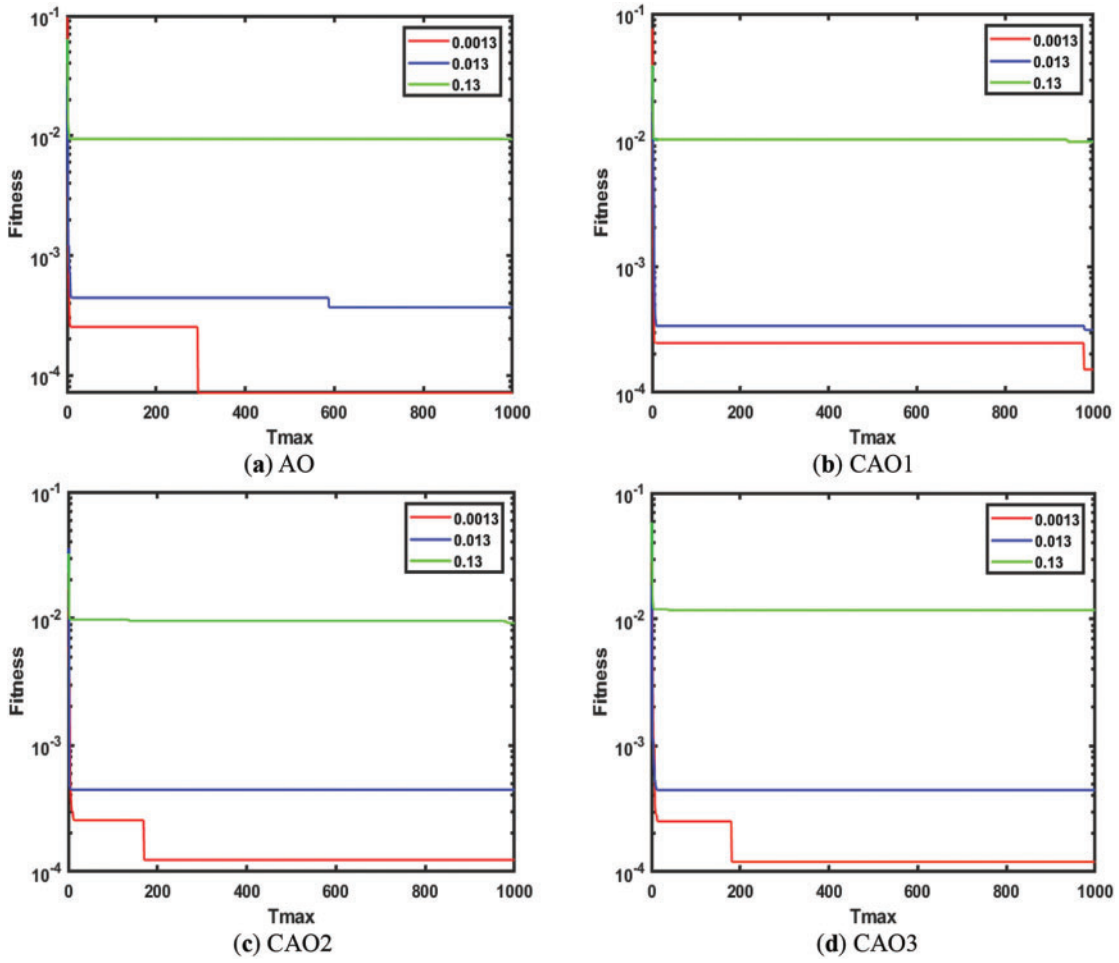


**Figure 7:** (Continued)

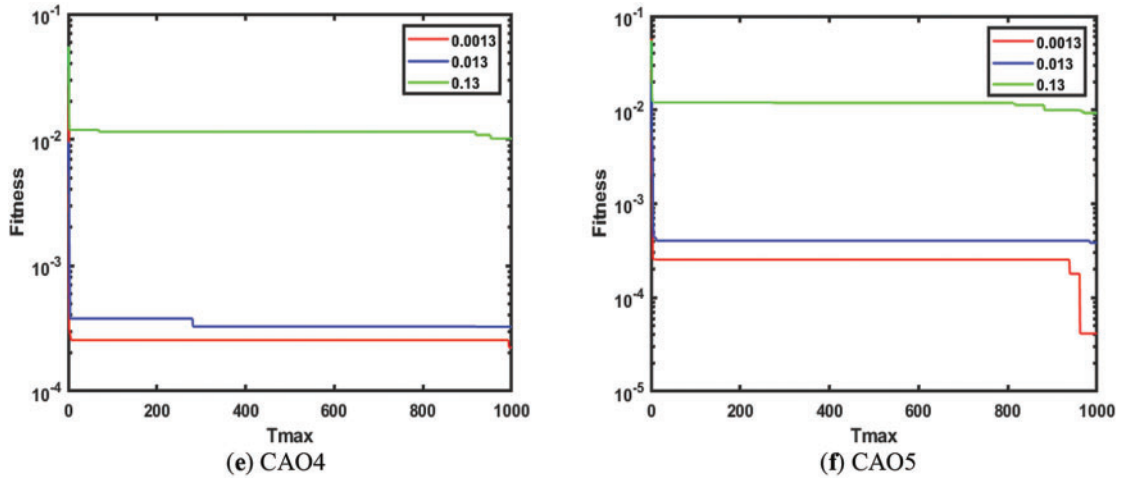


**Figure 7:** Performance of AO, and CAO1-5 for EHCS

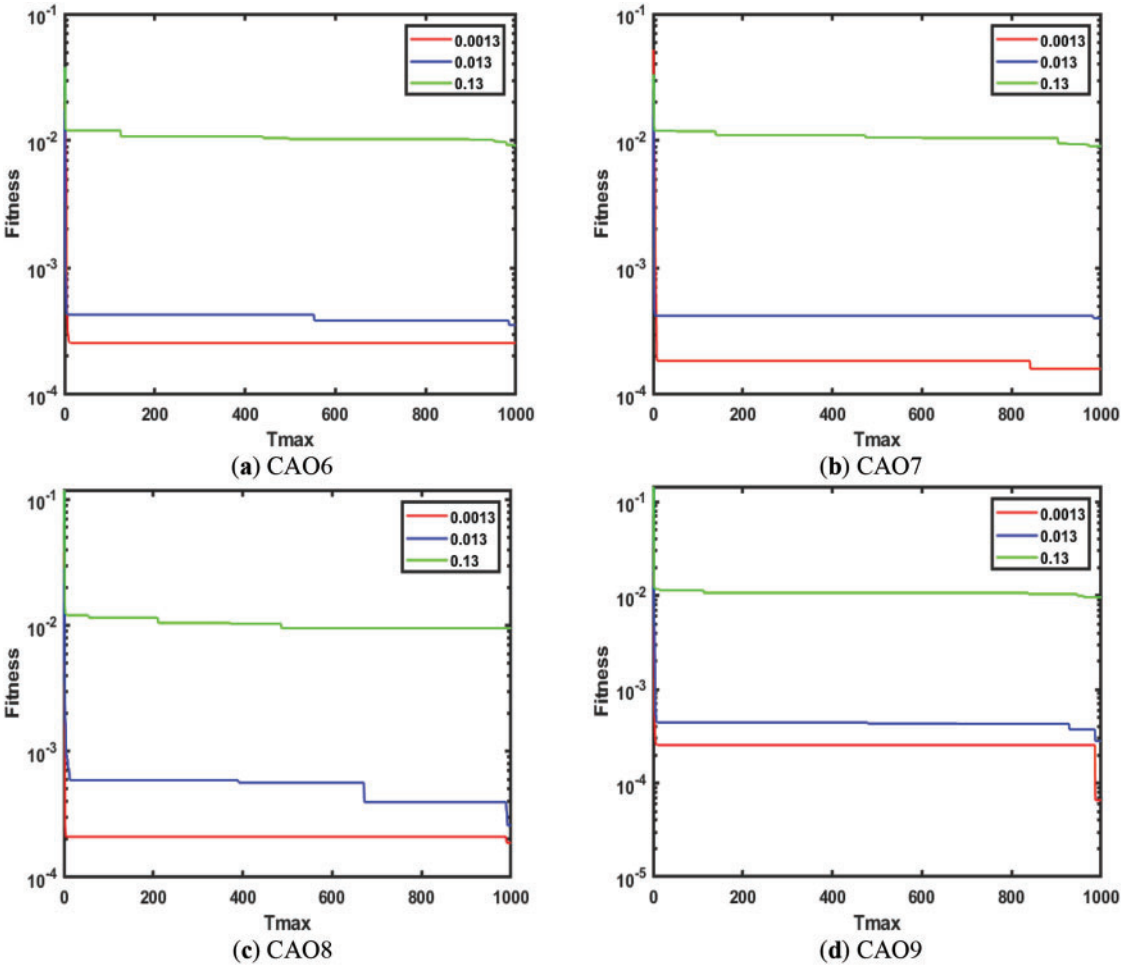


**Figure 8:** (Continued)

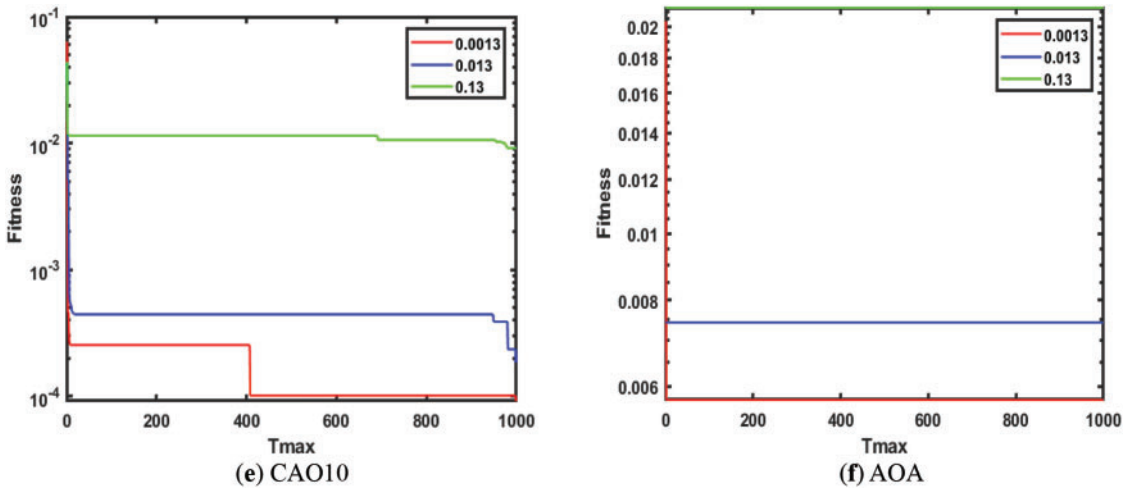


**Figure 8:** Performance of CAO6-10 and AOA for EHCS

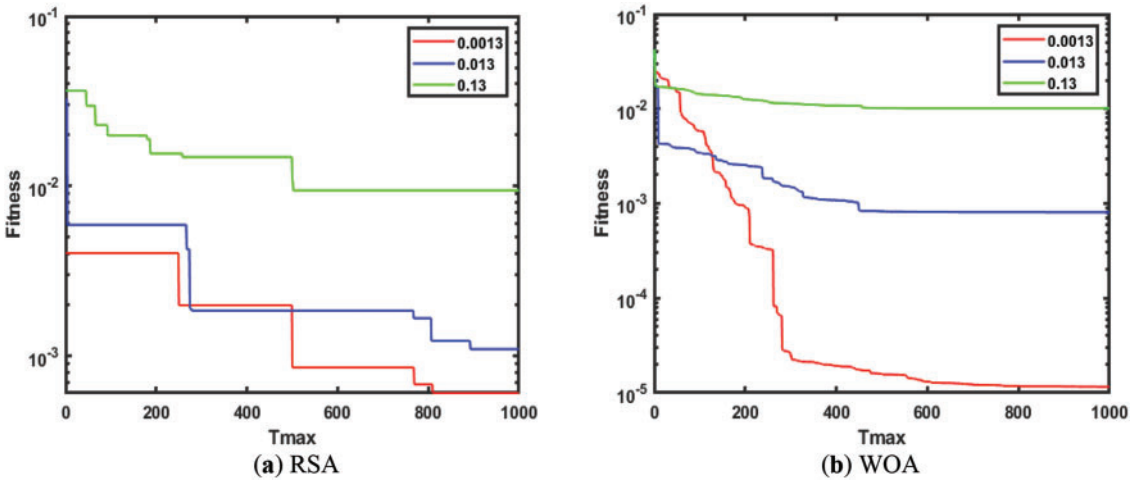


**Figure 9:** Performance of RSA and WOA for EHCS

Figs. 10 and 11 show the convergence plots of AO, AOA, CAO1-10, RSA, and WOA at $p_s$ = 12, 50, Tmax = 1000 and ρ (t) = [1.300E−01, 1.300E−02, 1.300E−03]. Fig. 10a–c shows the convergence for all OT's at $p_s$ = 12, whereas Fig. 11a–c shows the convergence at $p_s$ = 50. It is observed from Figs. 10 and 11 that CAO6 performs better for variations than AO, AOA, CAO1-5, CAO7-10, RSA, and WOA.

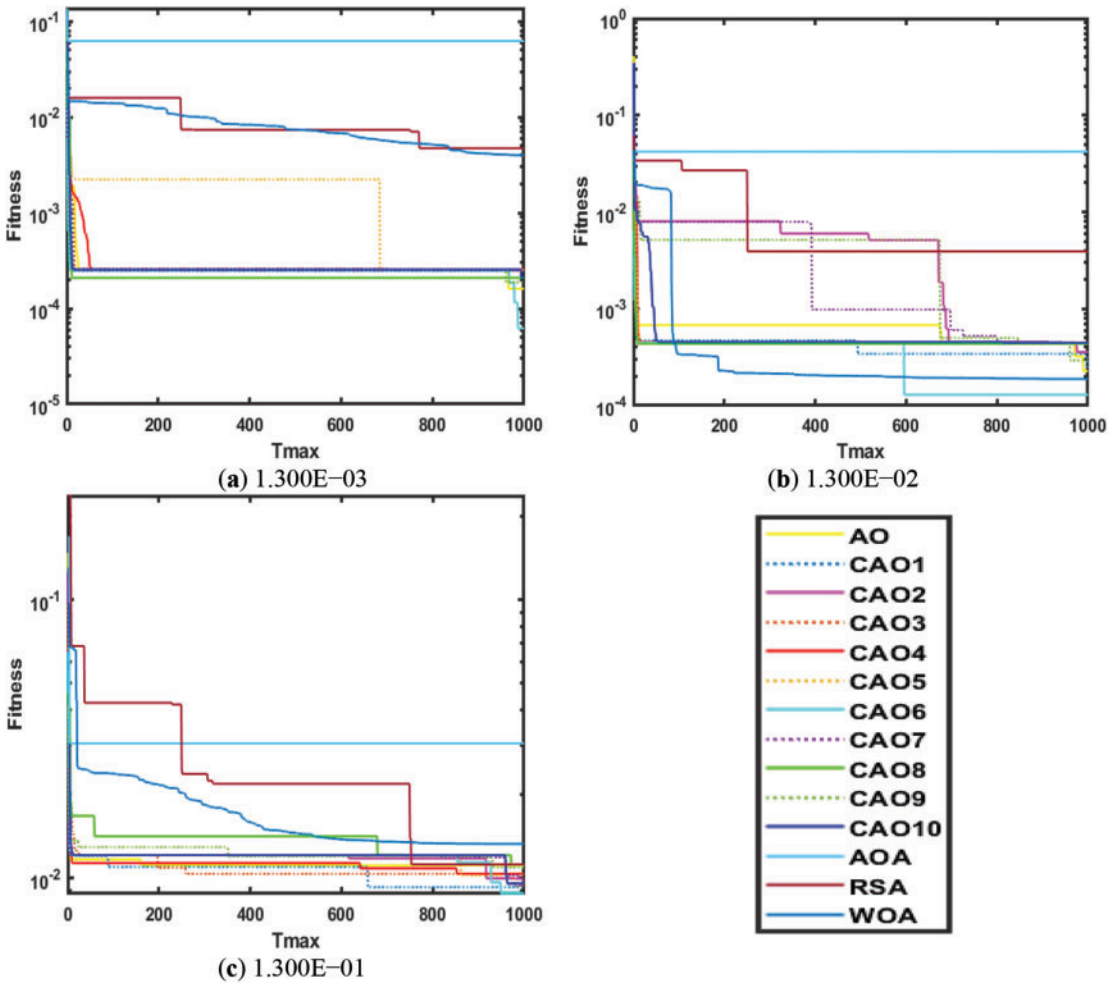


**Figure 10:** EHCS convergence analysis w.r.t noise at $p_s$ = 12

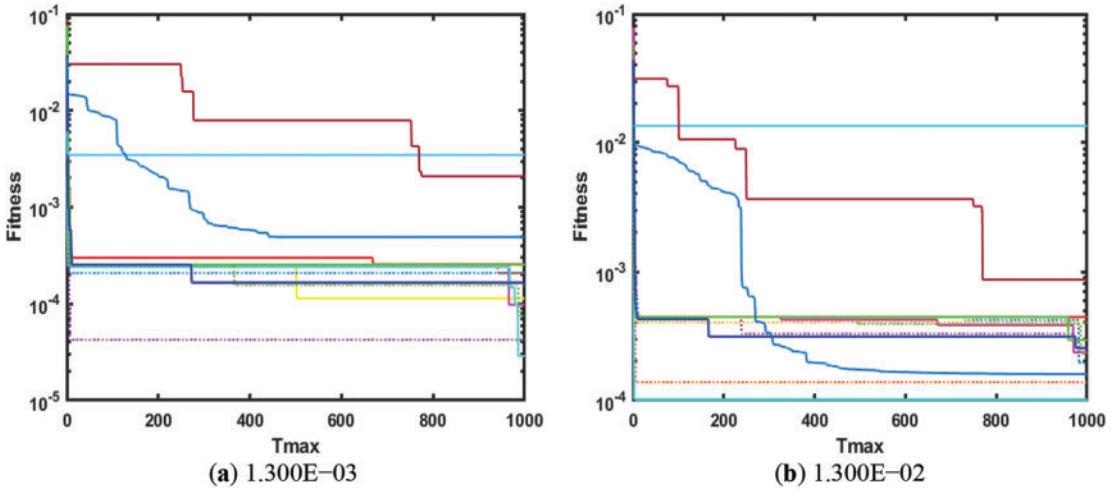


**Figure 11:** (Continued)

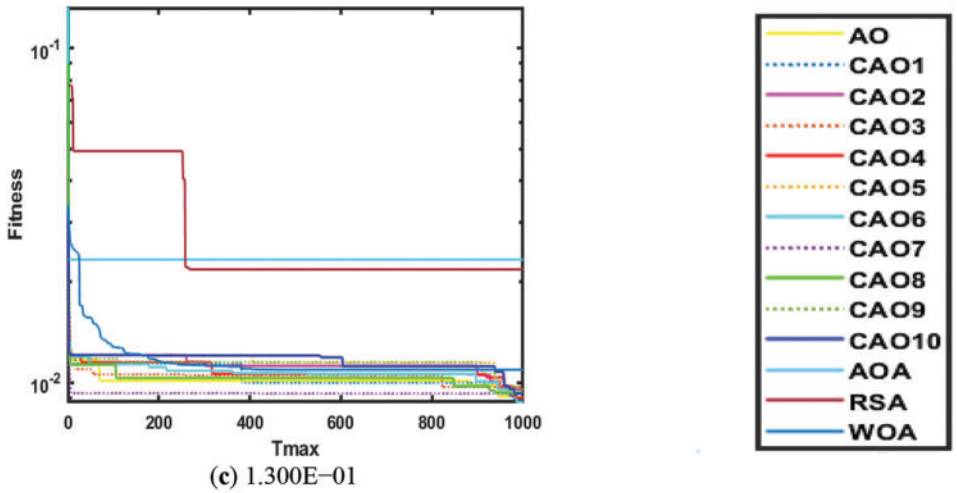


(c) 1.300E−01

**Figure 11:** EHCS convergence analysis w.r.t noise at $p_s$ = 50

The average computational time performance is measured on EHCS statistically on 100 independent runs at $p_s$ = 12, 50, Tmax = 1000 and $\rho(t)$ = 1.300E−03 as shown in Tables 13 and 14. In Tables 13 and 14, it is observed that for all OT's computational time increases when $p_s$ increases. However, CAO1-10 achieves a similar average computational time while maintaining the lowest fitness.

**Table 13:** Average computational time of AOA, AO, CAO1, CAO2, CAO3, CAO4 and CAO5 on EHCS

| $p_s$ | Noise | AOA | AO | CAO1 | CAO2 | CAO3 | CAO4 | CAO5 |
|---|---|---|---|---|---|---|---|---|
| 12 | 1.300E−03 | 2.024E+00 | 3.641E+00 | 3.662E+00 | 3.658E+00 | 3.733E+00 | 3.688E+00 | 3.679E+00 |
| 50 | 1.300E−03 | 7.110E+00 | 1.389E+01 | 1.388E+01 | 1.384E+01 | 2.029E+01 | 1.387E+01 | 1.382E+01 |

**Table 14:** Average computational time of CAO6, CAO7, CAO8, CAO9, CAO10, RSA and WOA on EHCS

| $p_s$ | Noise | CAO6 | CAO7 | CAO8 | CAO9 | CAO10 | RSA | WOA |
|---|---|---|---|---|---|---|---|---|
| 12 | 1.300E−03 | 3.671E+00 | 3.668E+00 | 3.677E+00 | 3.664E+00 | 3.731E+00 | 2.307E+00 | 2.022E+00 |
| 50 | 1.300E−03 | 1.387E+01 | 1.397E+01 | 1.386E+01 | 1.377E+01 | 1.383E+01 | 8.787E+00 | 7.066E+00 |

The average fitness of AO, CAO1-10, AOA, RSA, and WOA for EHCS is shown in Fig. 12. It is observed from Fig. 12 that CAO6 achieves the lowest average fitness against AO, CAO1-5, CAO7-10, AOA, RSA, and WOA.


**Figure 12:** Average fitness of all OT's w.r.t $p_s$ and $\rho$ (t) for EHCS

To further assess the performance, the Friedman Test for repeated measures [72] is executed on average fitness values of CAO6, AO, AOA, RSA, and WOA with a significance level of 5.000E−02. The obtained *p*-value is 1.100E−04, indicating that CAO6 is statistically significant.

Figs. 13–15 show the Taguchi test [86] analysis of AO, CAO1-10, AOA, RSA, and WOA for EHCS at $p_s$ = 12, 50, Tmax = 1000 and $\rho$ (t) = 1.300E−03. Fig. 13a–f shows the results for AO, CAO1, CAO2, CAO3, CAO4 and CAO5. Similarly, Figs. 14a–f and 15a,b show the convergence for CAO6, CAO7, CAO8, CAO9, CAO10, AOA, RSA, and WOA, respectively. It is prominent from Figs. 13–15 that for all OT's, S/N increases when $p_s$ is maximum.

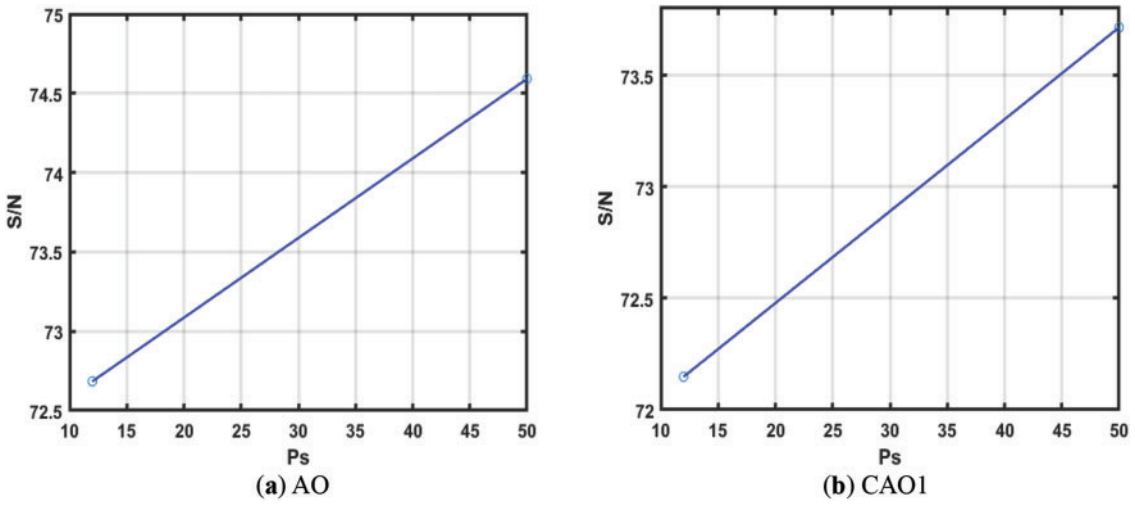


**Figure 13:** (Continued)

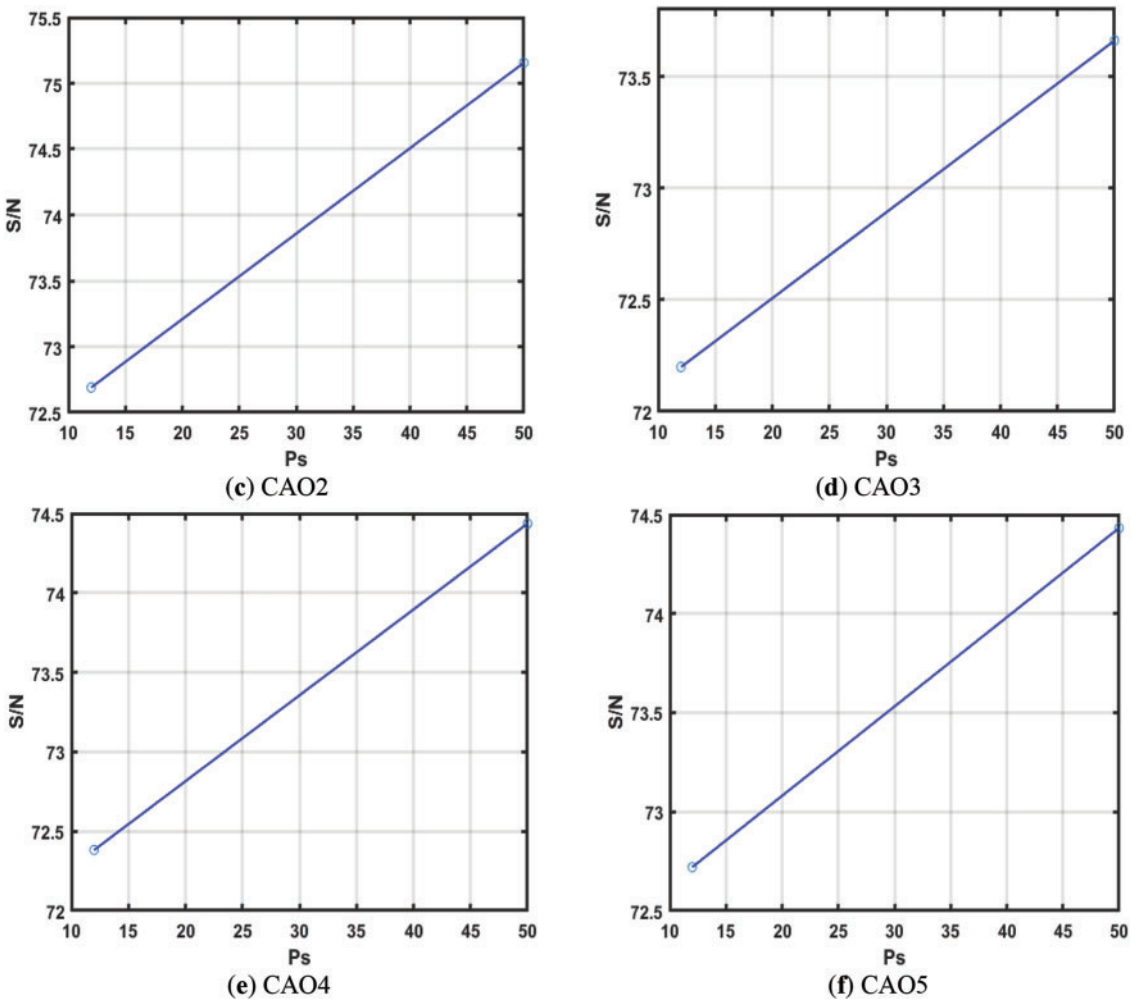


**Figure 13:** Taguchi analysis of AO, CAO1, CAO2, CAO3, CAO4 and CAO5 w.r.t $p_s$ for EHCS

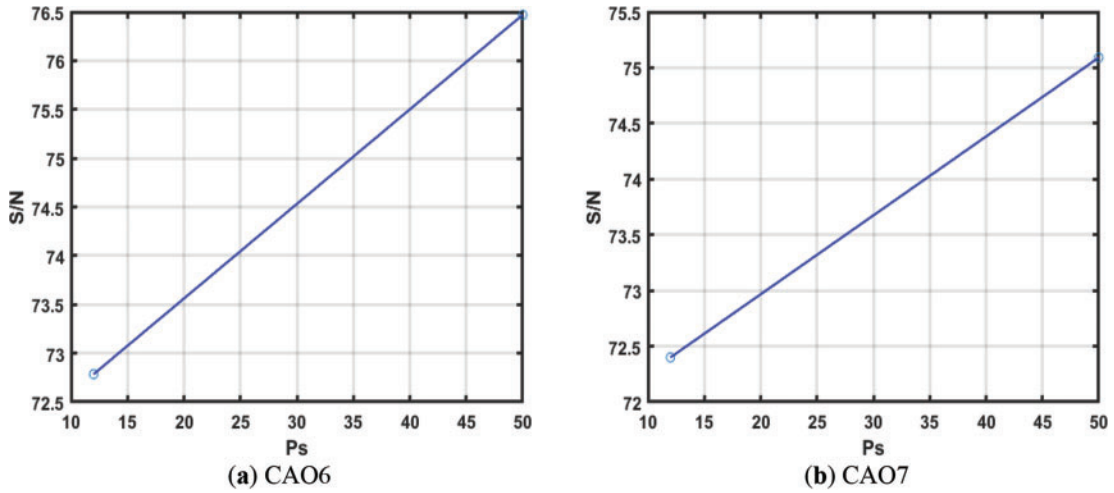


**Figure 14:** (Continued)

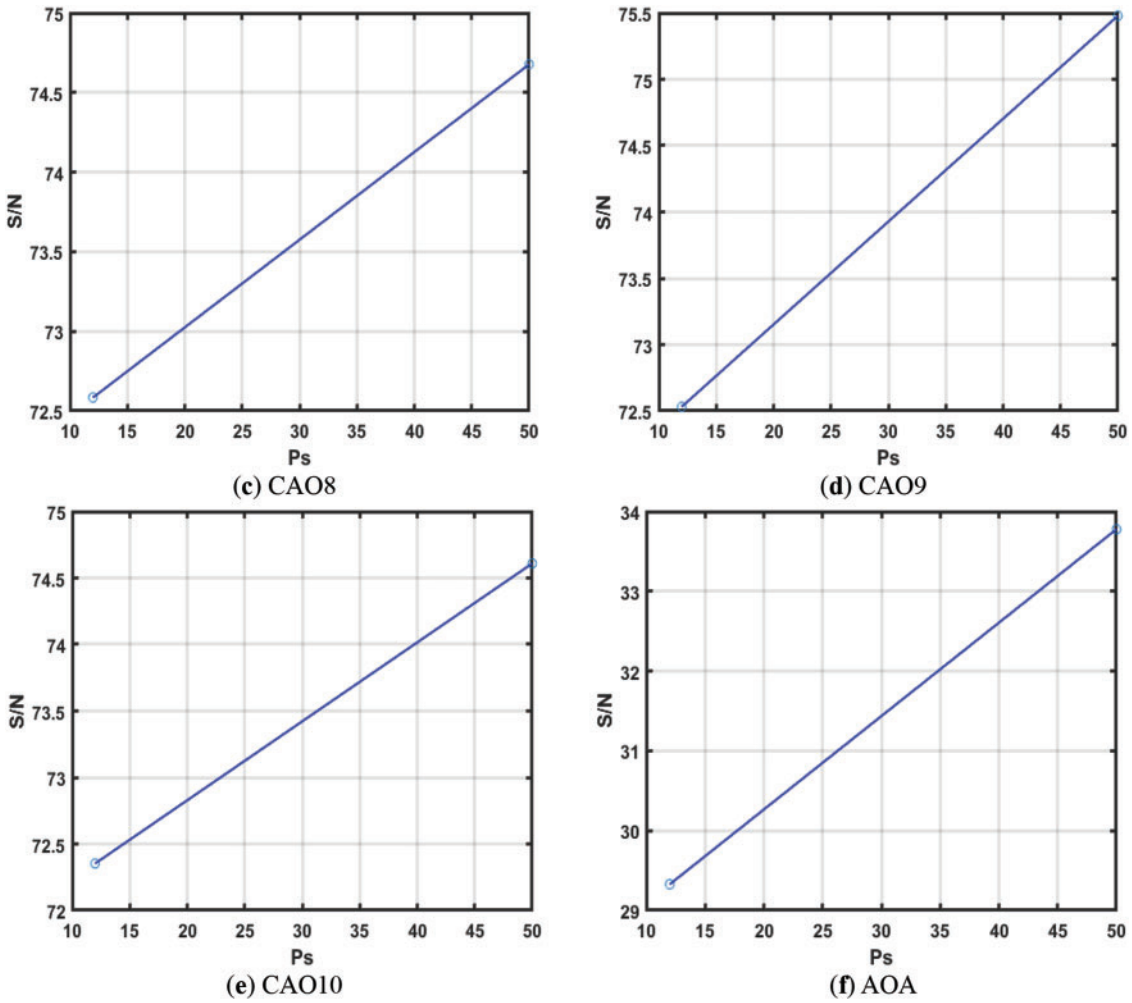


**Figure 14:** Taguchi analysis of CAO6, CAO7, CAO8, CAO9, CAO10 and AOA w.r.t $p_s$ for EHCS

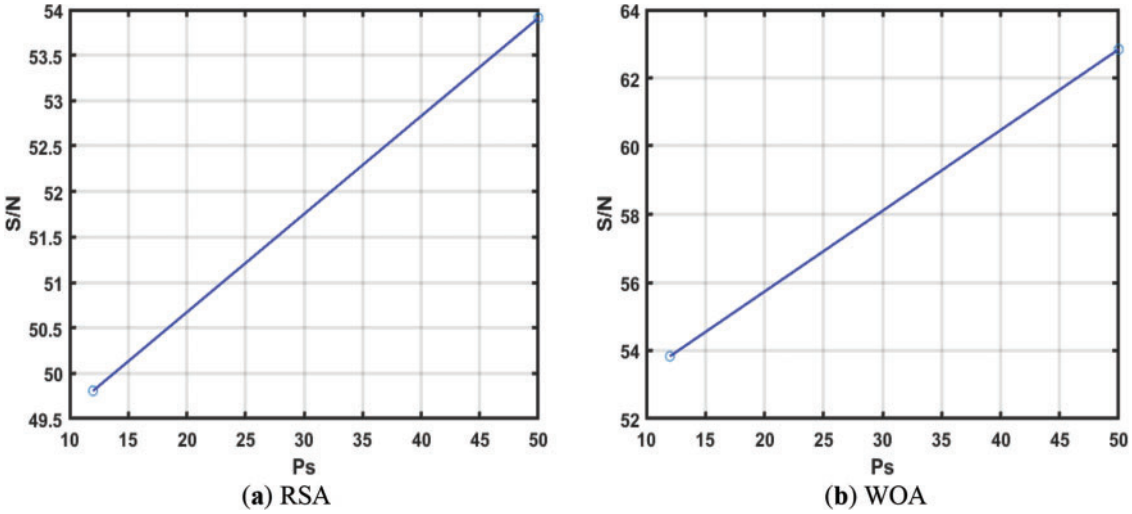


**Figure 15:** Taguchi analysis of RSA and WOA w.r.t $p_s$ for EHCS

## 5 Conclusion

In this work, an improved variant of AO is proposed by integrating ten well-known chaotic maps in a narrowed exploitation mechanism. The proposed variant is applied for the parameter estimation of the electro-hydraulic control system, EHCS. Statistical analysis, Taguchi test, computational analysis, and Friedman test for repeated measures verify that AO with a chaotic piecewise map (CAO6) performs better than AO, CAO1, CAO2, CAO3, CAO4, CAO5, CAO7, CAO8, CAO9, CAO10, AOA, RSA, and WOA for parameter estimation of EHCS model. The proposed study achieves significant results. However, it may suffer from sensitivity to parameter tuning, limiting its effectiveness in other optimization problems. Future research could explore hybridizing the Chaotic Aquila Optimizer (CAO) with machine learning assisted algorithms, and parameter tuning strategies to enhance performance in complex optimization problems with extension to solve real-world problems in areas like renewable energy, biomedical systems, and industrial process control automation.

**Acknowledgement:** The authors extend their appreciation to Taif University, Saudi Arabia, for supporting this project through project number (TU-DSPP-2024-52).

**Funding Statement:** This research was funded by Taif University, Saudi Arabia, Project No. (TU-DSPP-2024-52).

**Author Contributions:** Conceptualization, Khizer Mehmood and Naveed Ishtiaq Chaudhary; Writing—original draft, Khizer Mehmood; Writing—review and edit, Naveed Ishtiaq Chaudhary and Muhammad Asif Zahoor Raja; Validation, Naveed Ishtiaq Chaudhary and Zeshan Aslam Khan; Visualization, Khalid Mehmood Cheema, Kaled M. Alshmrany and Sultan S. Alshamrani; Formal analysis, Khizer Mehmood, Khalid Mehmood Cheema and Zeshan Aslam Khan; Funding acquisition, Sultan S. Alshamrani and Kaled M. Alshmrany; Project administration, Sultan S. Alshamrani and Kaled M. Alshmrany. All authors reviewed the results and approved the final version of the manuscript.

**Availability of Data and Materials:** Data sharing is not applicable to this article as no datasets were generated or analyzed during the current study.

**Ethics Approval:** Not applicable.

**Conflicts of Interest:** The authors declare no conflicts of interest to report regarding the present study.

## References

1. Li S, Zhou Y, Luo Q. Enhanced multi-object dwarf mongoose algorithm for optimization stochastic data fusion wireless sensor network deployment. Comput Model Eng Sci. 2025;142(2):1955–94. doi:10.32604/cmes.2025.059738.
2. Khan TA, Chaudhary NI, Hsu CC, Mehmood K, Khan ZA, Raja MAZ, et al. A gazelle optimization expedition for key term separated fractional nonlinear systems with application to electrically stimulated muscle modeling. Chaos Solitons Fractals. 2024;185(1):115111. doi:10.1016/j.chaos.2024.115111.
3. Das S, Rout SK, Panda SK, Mohapatra PK, Almazyad AS, Jasser MB, et al. Marine predators algorithm with deep learning-based leukemia cancer classification on medical images. Comput Model Eng Sci. 2024;141(1):893–916. doi:10.32604/cmes.2024.051856.
4. Mehmood K, Chaudhary NI, Khan ZA, Cheema KM, Raja MAZ. Parameter estimation of nonlinear systems: dwarf mongoose optimization algorithm with key term separation principle. J Ambient Intell Humaniz Comput. 2023;14(12):16921–31. doi:10.1007/s12652-023-04707-5.
5. Wang Y, Jin H, Wang GG, Wang L. A bi-population cooperative discrete differential evolution for multiobjective energy-efficient distributed blocking flow shop scheduling problem. IEEE Trans Syst Man Cybern Syst. 2025;55(3):2211–23. doi:10.1109/TSMC.2024.3520320.

6. Fatahi A, Nadimi-Shahraki MH, Zamani H. An improved binary quantum-based avian navigation optimizer algorithm to select effective feature subset from medical data: a COVID-19 case study. J Bionic Eng. 2024;21(1):426–46. doi:10.1007/s42235-023-00433-y.
7. Cheema KM, Mehmood K, Chaudhary NI, Khan ZA, Raja MAZ, El-Sherbeeny AM, et al. Knacks of marine predator heuristics for distributed energy source-based power systems harmonics estimation. Heliyon. 2024;10(15):e35776. doi:10.1016/j.heliyon.2024.e35776.
8. Song H, Wang J, Bei J, Wang M. Modified snake optimizer based multi-level thresholding for color image segmentation of agricultural diseases. Expert Syst Appl. 2024;255(8):124624. doi:10.1016/j.eswa.2024.124624.
9. Cheema KM, Mehmood K, Chaudhary NI, Khan ZA, Raja MAZ. A nadeem, Knacks of evolutionary mating heuristics for renewable energy source-based power systems signal harmonics estimation. Int J Energy Res. 2024;1(1):8871266. doi:10.1155/2024/8871266.
10. Wu Q, Cao Y, Wang H, Hong W. Machine-learning-assisted optimization and its application to antenna designs: opportunities and challenges. China Commun. 2020;17(4):152–64. doi:10.23919/JCC.2020.04.014.
11. Akinsolu MO, Mistry KK, Liu B, Lazaridis PI, Excell P. Machine learning-assisted antenna design optimization: a review and the state-of-the-art. In: Proceedings of the 2020 14th European Conference on Antennas and Propagation (EuCAP); 2020 Mar 15–20; Copenhagen, Denmark. doi:10.23919/EuCAP48036.2020.9135936.
12. Wu Q, Chen W, Yu C, Wang H, Hong W. Machine-learning-assisted optimization for antenna geometry design. IEEE Trans Antennas Propag. 2024;72(3):2083–95. doi:10.1109/TAP.2023.3346493.
13. Xu Y, Wandelt S, Sun X, Yang Y, Jin X, Karichery S, et al. Machine-learning-assisted optimization of aircraft trajectories under realistic constraints. J Guid Control Dyn. 2023;46(9):1814–25. doi:10.2514/1.G007038.
14. Bhatasana M, Marconnet A. Machine-learning assisted optimization strategies for phase change materials embedded within electronic packages. Appl Therm Eng. 2021;199(17–18):117384. doi:10.1016/j.applthermaleng.2021.117384.
15. Abualigah L, Sheikhan A, Ikotun AM, Zitar RA, Alsoud AR, Al-Shourbaji I, et al. Particle swarm optimization algorithm: review and applications. Metaheuristic Optim Algorithms. 2024;1–14. doi:10.1016/B978-0-443-13925-3.00019-4.
16. Wang GG, Deb S, Cui Z. Monarch butterfly optimization. Neural Comput Appl. 2019;31(7):1995–2014. doi:10.1007/s00521-015-1923-y.
17. Abualigah L, Elaziz MA, Sumari P, Geem ZW, Gandomi AH. Reptile search algorithm (RSA): a nature-inspired meta-heuristic optimizer. Expert Syst Appl. 2022;191(11):116158. doi:10.1016/j.eswa.2021.116158.
18. Mirjalili S, Lewis A. The whale optimization algorithm. Adv Eng Softw. 2016;95(12):51–67. doi:10.1016/j.advengsoft.2016.01.008.
19. Alzoubi S, Abualigah L, Sharaf M, Daoud MS, Khodadadi N, Jia H. Synergistic swarm optimization algorithm. Comput Model Eng Sci. 2024;139(3):2557–604. doi:10.32604/cmes.2023.045170.
20. Price KV. Differential evolution. In: Zelinka I, Snášel V, Abraham A, editors. Handbook of optimization. Berlin/Heidelberg, Germany: Springer; 2013. p. 187–214. doi:10.1007/978-3-642-30504-7_8.
21. Özcan N, Utku S, Berber T. Artificial circulation system algorithm: a novel bio-inspired algorithm. Comput Model Eng Sci. 2025;142(1):635–63. doi:10.32604/cmes.2024.055860.
22. Simon D. Biogeography-based optimization. IEEE Trans Evol Comput. 2008;12(6):702–13. doi:10.1109/TEVC.2008.919004.
23. Wang GG, Deb S, Coelho LDS. Earthworm optimisation algorithm: a bio-inspired metaheuristic algorithm for global optimisation problems. Int J Bio-Inspired Comput. 2018;12(1):1–22. doi:10.1504/IJBIC.2018.093328.
24. Wang GG. Moth search algorithm: a bio-inspired metaheuristic algorithm for global optimization problems. Memetic Comput. 2018;10(2):151–64. doi:10.1007/s12293-016-0212-3.
25. Abualigah L, Diabat A, Mirjalili S, Abd Elaziz M, Gandomi AH. The arithmetic optimization algorithm. Comput Methods Appl Mech Eng. 2021;376(2):113609. doi:10.1016/j.cma.2020.113609.
26. Bai J, Li Y, Zheng M, Khatir S, Benaissa B, Abualigah L, et al. A Sinh Cosh optimizer. Knowl-Based Syst. 2023;282(1):111081. doi:10.1016/j.knosys.2023.111081.

27. Mirjalili S, Mirjalili SM, Hatamlou A. Multi-verse optimizer: a nature-inspired algorithm for global optimization. Neural Comput Appl. 2016;27(2):495–513. doi:10.1007/s00521-015-1870-7.
28. Rashedi E, Nezamabadi-pour H, Saryazdi S. GSA: a gravitational search algorithm. Inf Sci. 2009;179(13):2232–48. doi:10.1016/j.ins.2009.03.004.
29. Hashim FA, Houssein EH, Mabrouk MS, Al-Atabany W, Mirjalili S. Henry gas solubility optimization: a novel physics-based algorithm. Future Gener Comput Syst. 2019;101(4):646–67. doi:10.1016/j.future.2019.07.015.
30. Askari Q, Younas I, Saeed M. Political optimizer: a novel socio-inspired meta-heuristic for global optimization. Knowl-Based Syst. 2020;195(5):105709. doi:10.1016/j.knosys.2020.105709.
31. Emami H. Stock exchange trading optimization algorithm: a human-inspired method for global optimization. J Supercomput. 2022;78(2):2125–74. doi:10.1007/s11227-021-03943-w.
32. Rao RV, Savsani VJ, Vakharia DP. Teaching-learning-based optimization: a novel method for constrained mechanical design optimization problems. Comput-Aided Des. 2011;43(3):303–15. doi:10.1016/j.cad.2010.12.015.
33. Askari Q, Saeed M, Younas I. Heap-based optimizer inspired by corporate rank hierarchy for global optimization. Expert Syst Appl. 2020;161(3):113702. doi:10.1016/j.eswa.2020.113702.
34. Elsisi M. Future search algorithm for optimization. Evol Intell. 2019;12(1):21–31. doi:10.1007/s12065-018-0172-2.
35. Abualigah L, Yousri D, Abd Elaziz M, Ewees AA, Al-qaness MAA, Gandomi AH. Aquila optimizer: a novel meta-heuristic optimization algorithm. Comput Ind Eng. 2021;157(11):107250. doi:10.1016/j.cie.2021.107250.
36. Sasmal B, Hussien AG, Das A, Dhal KG. A comprehensive survey on Aquila optimizer. Arch Comput Methods Eng. 2023;30(7):4449–76. doi:10.1007/s11831-023-09945-6.
37. Ahmadipour M, Murtadha Othman M, Bo R, Sadegh Javadi M, Mohammed Ridha H, Alrifaey M. Optimal power flow using a hybridization algorithm of arithmetic optimization and Aquila optimizer. Expert Syst Appl. 2024;235(4):121212. doi:10.1016/j.eswa.2023.121212.
38. Ateeq Almutairi S. An optimized feature selection and hyperparameter tuning framework for automated heart disease diagnosis. Comput Syst Sci Eng. 2023;47(2):2599–624. doi:10.32604/csse.2023.041609.
39. Alnfiai MM, Almalki N, Al-Wesabi FN, Alduhayyem M, Mustafa Hilal A, Ahmed Hamza M. Deep learning driven arabic text to speech synthesizer for visually challenged people. Intell Autom Soft Comput. 2023;36(3):2639–52. doi:10.32604/iasc.2023.034069.
40. Ramachandran A, Gayathri K, Alkhayyat A, Malik RQ. Aquila optimization with machine learning-based anomaly detection technique in cyber-physical systems. Comput Syst Sci Eng. 2023;46(2):2177–94. doi:10.32604/csse.2023.034438.
41. Agarwal N, Gokilavani M, Nagarajan S, Saranya S, Alsolai H, Dhahbi S, et al. Intelligent Aquila optimization algorithm-based node localization scheme for wireless sensor networks. Comput Mater Contin. 2023;74(1):141–52. doi:10.32604/cmc.2023.030074.
42. Alghazzawi DM, Hamid Hasan S, Bhatia S. Optimized generative adversarial networks for adversarial sample generation. Comput Mater Contin. 2022;72(2):3877–97. doi:10.32604/cmc.2022.024613.
43. Kari T, He Z, Rouzi A, Zhang Z, Ma X, Du L. Power transformer fault diagnosis using random forest and optimized kernel extreme learning machine. Intell Autom Soft Comput. 2023;37(1):691–705. doi:10.32604/iasc.2023.037617.
44. Gouri Tekkali C, Natarajan K. Smart fraud detection in E-transactions using synthetic minority oversampling and binary Harris Hawks optimization. Comput Mater Contin. 2023;75(2):3171–87. doi:10.32604/cmc.2023.036865.
45. Mehmood K, Chaudhary NI, Khan ZA, Raja MAZ, Cheema KM, Milyani AH. Design of Aquila optimization heuristic for identification of control autoregressive systems. Mathematics. 2022;10(10):1749. doi:10.3390/math10101749.
46. Alahmari S, Yonbawi S, Racharla S, Laxmi Lydia E, Khairi Ishak M, Khalid Alkahtani H, et al. Hybrid multi-strategy Aquila optimization with deep learning driven crop type classification on hyperspectral images. Comput Syst Sci Eng. 2023;47(1):375–91. doi:10.32604/csse.2023.036362.
47. Zhou Y, Chen Z, Gong Z, Chen P, Razmjooy S. The improved Aquila optimization approach for cost-effective design of hybrid renewable energy systems. Heliyon. 2024;10(6):e27281. doi:10.1016/j.heliyon.2024.e27281.

48. Rajinikanth V, Mohamed Aslam S, Kadry S, Thinnukool O. Semi/fully-automated segmentation of gastric-polyp using Aquila-optimization-algorithm enhanced images. Comput Mater Contin. 2022;70(2):4087–105. doi:10.32604/cmc.2022.019786.
49. Ekinci S, Izci D, Abualigah L, Zitar RA. A modified oppositional chaotic local search strategy based Aquila optimizer to design an effective controller for vehicle cruise control system. J Bionic Eng. 2023;20(4):1828–51. doi:10.1007/s42235-023-00336-y.
50. Ekinci S, Izci D, Eker E, Abualigah L. An effective control design approach based on novel enhanced Aquila optimizer for automatic voltage regulator. Artif Intell Rev. 2023;56(2):1731–62. doi:10.1007/s10462-022-10216-2.
51. Ma Y, Shao P, Liu X, Wang L. Collaborative trajectory planning for stereoscopic agricultural multi-UAVs driven by the Aquila optimizer. Comput Mater Contin. 2025;82(1):1349–76. doi:10.32604/cmc.2024.058294.
52. Ekinci S, Izci D, Abualigah L. A novel balanced Aquila optimizer using random learning and Nelder-Mead simplex search mechanisms for air-fuel ratio system control. J Braz Soc Mech Sci Eng. 2023;45(1):68. doi:10.1007/s40430-022-04008-6.
53. An D, Jia J, Cai W, Yang D, Lv C, Zhu J, et al. A novel Aquila optimizer based pv array reconfiguration scheme to generate maximum energy under partial shading condition. Energy Eng. 2022;119(4):1531–45. doi:10.32604/ee.2022.019284.
54. Cavlak Y, Ateş A, Abualigah L, Elaziz MA. Fractional-order chaotic oscillator-based Aquila optimization algorithm for maximization of the chaotic with Lorentz oscillator. Neural Comput Appl. 2023;35(29):21645–62. doi:10.1007/s00521-023-08945-8.
55. Baş E. Binary Aquila optimizer for 0–1 knapsack problems. Eng Appl Artif Intell. 2023;118(22):105592. doi:10.1016/j.engappai.2022.105592.
56. Turgut E, Turgut MS. Local search enhanced Aquila optimization algorithm ameliorated with an ensemble of wavelet mutation strategies for complex optimization problems. Math Comput Simul. 2023;206:302–74. doi:10.1016/j.matcom.2022.11.020.
57. Liu H, Zhang X, Zhang H, Li C, Chen Z. A reinforcement learning-based hybrid Aquila optimizer and improved arithmetic optimization algorithm for global optimization. Expert Syst Appl. 2023;224(11):119898. doi:10.1016/j.eswa.2023.119898.
58. Verma M, Sreejeth M, Singh M, Babu TS, Alhelou HH. Chaotic mapping based advanced Aquila optimizer with single stage evolutionary algorithm. IEEE Access. 2022;10(4):89153–69. doi:10.1109/ACCESS.2022.3200386.
59. Zhang Y, Xu X, Zhang N, Zhang K, Dong W, Li X. Adaptive Aquila optimizer combining niche thought with dispersed chaotic swarm. Sensors. 2023;23(2):755. doi:10.3390/s23020755.
60. Wang Y, Xiao Y, Guo Y, Li J. Dynamic chaotic opposition-based learning-driven hybrid Aquila optimizer and artificial rabbits optimization algorithm: framework and applications. Processes. 2022;10(12):2703. doi:10.3390/pr10122703.
61. Yang M, Yan G, Zhang Y, Zhang T, Ai C. Research on high efficiency and high dynamic optimal matching of the electro-hydraulic servo pump control system based on NSGA-II. Heliyon. 2023;9(3):e13805. doi:10.1016/j.heliyon.2023.e13805.
62. Ling TG, Rahmat MF, Husain AR. System identification and control of an electro-hydraulic actuator system. In: Proceedings of the 2012 IEEE 8th International Colloquium on Signal Processing and its Applications; 2012 Mar 23–25; Malacca, Malaysia. doi:10.1109/CSPA.2012.6194696.
63. Liang XW, Faudzi AAM, Ismail ZH. System identification and model predictive control using CVXGEN for electro-hydraulic actuator. Int J Integr Eng. 2019;11(4):166–74. doi:10.30880/ijie.2019.11.04.018.
64. Izzuddin NH, Faudzi AAM, Johari MR, Osman K. System identification and predictive functional control for electro-hydraulic actuator system. In: Proceedings of the 2015 IEEE International Symposium on Robotics and Intelligent Sensors (IRIS); 2015 Oct 18–20; Langkawi, Malaysia. doi:10.1109/IRIS.2015.7451600.
65. Mehmood K, Chaudhary NI, Cheema KM, Khan ZA, Raja MAZ, Milyani AH, et al. Design of nonlinear marine predator heuristics for Hammerstein autoregressive exogenous system identification with key-term separation. Mathematics. 2023;11(11):2512. doi:10.3390/math11112512.

66. Ding F, Lv L, Pan J, Wan X, Jin XB. Two-stage gradient-based iterative estimation methods for controlled autoregressive systems using the measurement data. Int J Control Autom Syst. 2020;18(4):886–96. doi:10.1007/s12555-019-0140-3.
67. Li F, Zheng T, He N, Cao Q. Data-driven hybrid neural fuzzy network and ARX modeling approach to practical industrial process identification. IEEE/CAA J Autom Sin. 2022;9(9):1702–5. doi:10.1109/JAS.2022.105821.
68. Mehmood K, Chaudhary NI, Khan ZA, Cheema KM, Raja MAZ, Milyani AH, et al. Dwarf mongoose optimization metaheuristics for autoregressive exogenous model identification. Mathematics. 2022;10(20):3821. doi:10.3390/math10203821.
69. Tu Q, Rong Y, Chen J. Parameter identification of ARX models based on modified momentum gradient descent algorithm. Complexity. 2020;1(3):9537075. doi:10.1155/2020/9537075.
70. Wu J, Wang F, Xu B, Sun Z. Characteristics study of electro-hydraulic load-sensing control system for mobile machines. Proc Inst Mech Eng Part J Automob Eng. 2023;237(9):2344–54. doi:10.1177/09544070221105386.
71. Alatas B. Chaotic harmony search algorithms. Appl Math Comput. 2010;216(9):2687–99. doi:10.1016/j.amc.2010.03.114.
72. Mehmood K, Khan ZA, Chaudhary NI, Cheema KM, Siddiqui B, Raja MAZ. Design of chaotic Young's double slit experiment optimization heuristics for identification of nonlinear muscle model with key term separation. Chaos Solitons Fractals. 2024;189(20):115636. doi:10.1016/j.chaos.2024.115636.
73. Turgut E, Turgut MS, Kırtepe E. Chaotic Aquila optimization algorithm for solving phase equilibrium problems and parameter estimation of semi-empirical models. J Bionic Eng. 2024;21(1):486–526. doi:10.1007/s42235-023-00438-7.
74. Mehmood K, Chaudhary NI, Khan ZA, Cheema KM, Raja MAZ, Shu CM. Novel knacks of chaotic maps with Archimedes optimization paradigm for nonlinear ARX model identification with key term separation. Chaos Solitons Fractals. 2023;175(3):114028. doi:10.1016/j.chaos.2023.114028.
75. Wang GG, Guo L, Gandomi AH, Hao GS, Wang H. Chaotic krill herd algorithm. Inf Sci. 2014;274(2):17–34. doi:10.1016/j.ins.2014.02.123.
76. Alatas B. Chaotic bee colony algorithms for global numerical optimization. Expert Syst Appl. 2010;37(8):5682–7. doi:10.1016/j.eswa.2010.02.042.
77. Turgut E, Turgut MS. Chaotic gradient based optimizer for solving multidimensional unconstrained and constrained optimization problems. Evol Intell. 2024;17(3):1967–2028. doi:10.1007/s12065-023-00876-6.
78. Mehmood K, Chaudhary NI, Khan ZA, Cheema KM, Raja MAZ. Variants of chaotic grey wolf heuristic for robust identification of control autoregressive model. Biomimetics. 2023;8(2):141. doi:10.3390/biomimetics8020141.
79. Gezici H, Livatyalı H. Chaotic harris hawks optimization algorithm. J Comput Des Eng. 2022;9(1):216–45. doi:10.1093/jcde/qwab082.
80. Gharehchopogh FS, Nadimi-Shahraki MH, Barshandeh S, Abdollahzadeh B, Zamani H. CQFFA: a chaotic quasi-oppositional farmland fertility algorithm for solving engineering optimization problems. J Bionic Eng. 2023;20(1):158–83. doi:10.1007/s42235-022-00255-4.
81. Wang GG, Deb S, Gandomi AH, Zhang Z, Alavi AH. Chaotic cuckoo search. Soft Comput. 2016;20(9):3349–62. doi:10.1007/s00500-015-1726-1.
82. Mehmood K, Chaudhary NI, Khan ZA, Cheema KM, Zahoor Raja MA. Atomic physics-inspired atom search optimization heuristics integrated with chaotic maps for identification of electro-hydraulic actuator systems. Mod Phys Lett B. 2024;38(30):2450308. doi:10.1142/S0217984924503081.
83. Wang GG, Hossein Gandomi A, Hossein Alavi A. A chaotic particle-swarm krill herd algorithm for global numerical optimization. Kybernetes. 2013;42(6):962–78. doi:10.1108/K-11-2012-0108.
84. Elbayomy KM, Jiao ZX, Zhang HQ. PID controller optimization by GA and its performances on the electro-hydraulic servo control system. Chin J Aeronaut. 2008;21(4):378–84. doi:10.1016/S1000-9361(08)60049-7.
85. Yan J, Li B, Guo G, Zeng Y, Zhang M. Nonlinear modeling and identification of the electro-hydraulic control system of an excavator arm using BONL model. Chin J Mech Eng. 2013;26(6):1212–21. doi:10.3901/CJME.2013.06.1212.
86. Abedi Pahnehkolaei SM, Alfi A, Machado JAT. Particle swarm optimization algorithm using complex-order derivative concept: a comprehensive study. Appl Soft Comput. 2021;111(2):107641. doi:10.1016/j.asoc.2021.107641.